Performance of a Drifting Acoustic Instrumentation SYstem (DAISY) for Characterizing Radiated Noise from Marine Energy Converters

Brian Polagye[1,2*], Corey Crisp[1], Lindsey Jones[1], Paul Murphy[3], Jessica Noe[2], Gemma Calandra[1], Christopher Bassett[2]

[1*]Mechanical Engineering, University of Washington, 3900 E Stevens Way NE, Seattle, 98195-2600, WA, United States.
[2]Applied Physics Laboratory, University of Washington, 1013 NE 40[th] Street, Seattle, 98105-6698, WA, United States.
[3]MarineSitu, Inc., 909 Boat Street, Seattle, 98105, WA, United States.

*Corresponding author(s). E-mail(s): bpolagye@uw.edu;
Contributing authors: crispc85@gmail.com; ljones37@uw.edu; paul@marinesitu.com; noej@uw.edu; gcalan@uw.edu; cbassett@uw.edu;

Abstract

Marine energy converters can generate electricity from energetic ocean waves and water currents. Because sound is extensively used by marine animals, the radiated noise from these systems is of regulatory interest. However, the energetic nature of these locations poses challenges for performing accurate passive acoustic measurements, particularly with stationary platforms. The Drifting Acoustic Instrumentation SYstem (DAISY) is a modular hydrophone recording system purpose-built for marine energy environments. Using a flow shield in currents and mass-spring-damper suspension system in waves, we demonstrate that DAISYs can effectively minimize the masking effect of flow noise at frequencies down to 10 Hz. In addition, we show that groups of DAISYs can utilize time-delay-of-arrival post-processing to attribute radiated noise to a specific source. Consequently, DAISYs can rapidly measure radiated noise at all frequencies of interest for prototype marine energy converters. The resulting information from future operational deployments should support regulatory decision-making and allow technology developers to make design adjustments that minimize the potential for acoustic impacts as their systems are scaled up for utility-scale power generation.

Keywords: marine energy, underwater noise, passive acoustics, drifting hydrophone

1 Introduction

Waves and currents can be harnessed to generate renewable electricity and, like other forms of renewable energy generation, economic viability is tied to resource intensity. Consequently, utility-scale deployments of marine energy converters require locations with relatively high annual-average wave power flux (> 10 kW/m) for wave energy converters (WECs) and relatively high water speeds (> 1 m/s) for current turbines. To date, a limited number of marine energy converters have been deployed, demonstrating technological feasibility (Melikoglu, 2018), but widespread adoption requires cost reductions to achieve parity with more mature forms of energy generation.

This state of pre-converged technology affords an opportunity to identify potential environmental impacts and mitigate them by design. As with any anthropogenic activity in the marine environment, marine energy converter installation and operation can generate underwater noise, which is of regulatory interest because marine animals use sound for a variety of biological functions (Popper and Hastings, 2009; Richardson et al., 2013). Summaries of observations to date (e.g., Polagye and Bassett (2020)), suggest that marine energy converters primarily radiate mechanical noise from their power take-offs and mooring systems at frequencies less than 5 kHz. Depending on the configuration of the power take-off, radiated noise may be present at frequencies up to 10s of kHz (Risch et al., 2020). Because moving mechanical components are coupled directly to the water, at equivalent electrical power levels, WECs and current turbines tend to radiate higher intensity noise than offshore wind turbines (Tougaard et al., 2020). However, pile foundation installation, which has acute acoustic impacts for offshore wind (Amaral et al., 2020) is less common for WECs and current turbines. Consequently, regulatory concern for these technologies is less focused on mechanisms for acoustic injury than on the potential for behavioral alteration due to masking of natural sounds, attraction, or avoidance (Polagye and Bassett, 2020; Hasselman et al., 2023). The first step to identifying opportunities to mitigate potential acoustic impacts is a more thorough understanding of the characteristics of radiated noise (i.e., frequencies, intensities, temporal variability) from initial deployments of WECs and current turbines.

Stationary passive acoustic measurements using hydrophones mounted to a fixed platform are well-suited to understanding temporal variability and commonly used to study noise in marine environments (Sousa-Lima et al., 2013). However, this mode of observation faces two unique challenges for marine energy measurements. First, because prototype marine energy converters may be smaller than intended for their ultimate application, measurements at relatively close range may be necessary to accurately characterize the full spectrum of radiated noise. For fixed platforms, this can be difficult to achieve without risking mooring entanglement or collision with the marine energy converter during deployment and recovery. While such concerns can be obviated by coupling a hydrophone directly with the marine energy converter, this may place the sensor in a region where measurements are unrepresentative of the acoustic far-field, introduces potential for contamination by platform vibrations, and increases the risk of acoustic shadowing by the marine energy converter. Consequently, such measurements are biased in a way that complicates interpretation of radiated noise. Second, by necessity, marine energy converters are deployed in environments with significant water motion. Because of this, "flow noise"–the non-propagating pressure fluctuations arising from relative velocity between a hydrophone and surrounding water (Strasberg, 1979)–is omnipresent and can mask propagating sound at frequencies up to several hundred Hz (Bassett et al., 2014). This is meaningful because these masked frequencies may overlap with the radiated noise associated with marine energy conversion. While the occurrence of flow noise is relatively intuitive for measurements around turbines operating in river, tidal, and ocean currents, in energetic waves, water orbital velocities near the seabed can also generate appreciable flow noise. For example, in a water depth of 50 m, linear wave theory suggests that a 3 m wave height at a 12 s period would yield a maximum water velocity of 0.4 m/s near the seabed (Demirbilek and Vincent, 2002).

Both of these challenges are substantially mitigated by drifting hydrophones, which also offer two unique benefits. First, currents, waves, and wind transport the hydrophone over time, resulting in a progression of measurements at different ranges to a marine energy converter. In wave environments, measurements at ranges of interest are typically obtained in less than 30 minutes. For currents, drifts are faster, capturing relevant information in a few minutes. The spatial resolution of radiated noise and the relative ease with which this can be obtained are particularly helpful for reconnaissance purposes and can complement stationary measurements that characterize temporal variability (IEC, 2019). Second, because of the limited knowledge base for radiated noise from marine energy converters, source attribution can be difficult with a single hydrophone. For example, in Polagye et al. (2017) a persistent "warble" around a WEC was attributed to a failing bearing in a power take-off. However, a longer term measurement subsequently showed that this noise recurred after the WEC was removed and was actually attributable to an element of the mooring system. When groups of drifting hydrophones are deployed around a marine energy converter, time-delay-of-arrival methods (e.g., Watkins and Schevill (1972)) may be able to localize some types of radiated noise. The attribution is important because, to mitigate a problematic source of noise, the course of action for a technology developer is quite different if a sound is being radiated from an element of the power take-off versus an element of the mooring system.

Documented examples of drifting hydrophones used to characterize radiated noise from marine energy converters include:

- "Drifting Ears," a research-grade drifting hydrophone used to measure radiated noise from multiple tidal turbines (Wilson et al., 2014; Risch et al., 2020, 2023)
- A hydrophone suspended from an "anti-heave buoy" used to measure radiated noise around a tidal turbine (Lossent et al., 2018)
- A spar buoy modified by our research group to measure radiated noise from a WEC (Bassett et al., 2011) and river current turbine (Polagye and Murphy, 2015)

These systems have similarities to sonobuoys used in research and anti-submarine warfare (Holler, 2014) and hydrophone drifters for ecological monitoring (e.g., Pirotta et al. (2023)) in that they are intended to accurately identify sounds at relatively low frequencies in adverse wave conditions. Development of a new drifting system was motivated by three gaps. First, existing systems used in marine energy applications were not intended for localization and, as such, did not include GPS clock synchronization or hydrophone depth information. Second, there were limited benchmarks about how well existing systems mitigated masking from flow noise. Third, a more modular design could allow a basic system architecture to be used in both wave and current environments.

The objective of this paper is to describe the design considerations for a drifting hydrophone system purpose-built for measurements around marine energy converters, benchmark the effectiveness of this design to resolve sound at all frequencies of interest in energetic currents and waves, and demonstrate sound source localization when multiple units are used as a long baseline array. The remainder of this paper is structured as follows. Section 2 describes the general architecture and performance of the Drifting Acoustic Instrumentation SYstem (DAISY). Section 3 quantifies performance in currents, and Section 4 quantifies performance in waves. The ability of groups of DAISYs to localize sound is demonstrated in Section 5. We conclude with a brief summary of system performance and limitations. By intention, this paper does not include operational examples of noise measurements around marine energy converters. Such measurements are more appropriate for inclusion in standalone publications that are able to treat the topic in depth (e.g., Haxel et al. (2022)).

2 General Architecture

Our group's initial work with drifting hydrophones utilized a version of the SWIFT buoy designed for wave measurement (Thomson, 2012), retrofitted with a hydrophone at the base of the spar. This approach proved effective for currents (Polagye and Murphy, 2015) and limited waves (Bassett et al., 2011) but restricted the hydrophone depth to ∼1 m and generated unacceptably high flow noise and self noise in more energetic wave environments. In addition, collecting metadata about system performance (e.g., orientation, acceleration) required separate, autonomous sensors which were personnel-intensive to configure during field operations. At the same time, this metadata proved helpful in interpreting acoustic signals. With support from the U.S. Department of Energy's Triton Initiative (Chang et al., 2021; Eaves et al., 2022), we developed a new, modular system with integrated metadata collection. Over a six-year period, we had the opportunity to test performance in energetic waves and currents at multiple locations and iterate on the design.

2.1 Hardware

DAISYs consist of a surface expression, hydrophone recording package at depth, and an intermediate connection between the two. Because the intermediate connection varies between currents and waves, it is discussed in Sections 3 and 4, respectively.

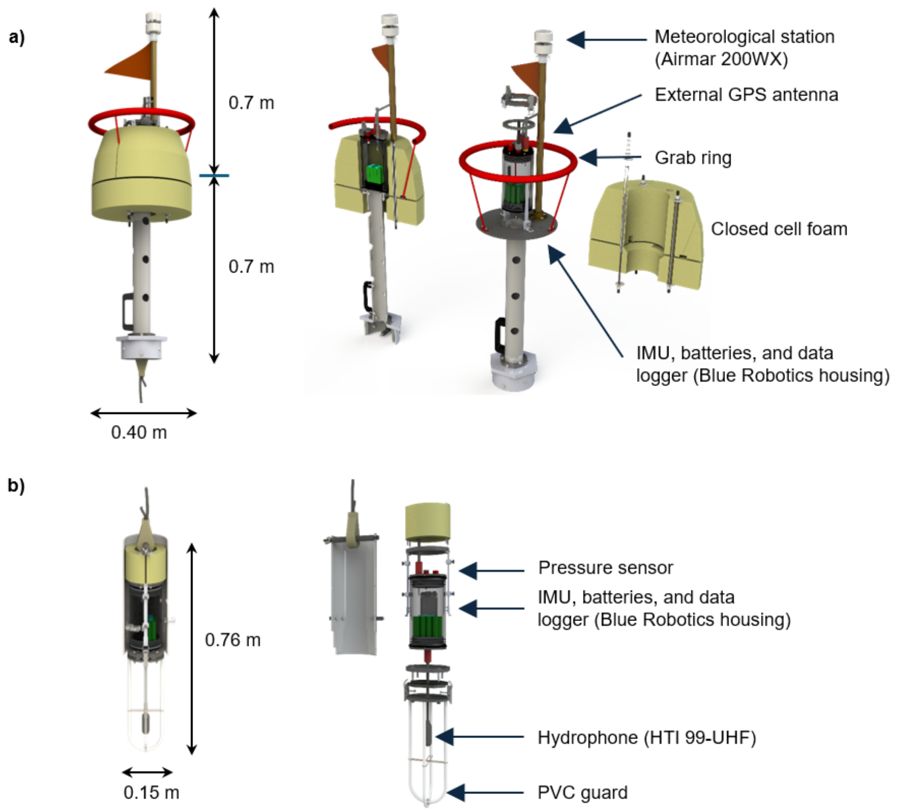

Fig. 1 Annotated exploded views of (a) DAISY surface expression and (b) DAISY hydrophone package. On the surface expression, the approximate waterline is indicated by the break in vertical dimension.

The surface expression (Fig. 1a) is a positively-buoyant spar buoy equipped with a nine degree of freedom (9-DOF) inertial measurement unit (EM7180 Motion Co-Processor w/ MPU9250 9-DOF IMU), global positioning system (uBlox NEO 7N GNSS module, 2.5m horizontal accuracy), and compact meteorological station (Airmar 200WX). Via a custom printed circuit board, these sensors are tied into a microcomputer (Beaglebone PocketBeagle) that ensures time synchronization across all sensors. The GPS (1 Hz) geo-references acoustic measurements, the IMU (25 Hz) evaluates surface expression motion relative to the hydrophone package, and the meteorological station (1 Hz) monitors dominant wind speed and direction during deployments. We considered incorporating a real-time kinematic (RTK) GPS, but this would have been more costly and would only have increased the accuracy of surface expression location, not the hydrophone, which has inherent ambiguity from the flexible tether. In addition, localization errors are dominated by uncertainty in signal arrival time and geometric constraints due to array orientation, not uncertainty in receiver position (Section 5). Where possible, physical hardware uses common, low-cost components, such as PVC pipe for the spar. The spar configuration, which incorporates closed cell foam at the surface and lead sheet in the base, generates a strong righting moment that maintains stability and limits the risk of submergence that could disrupt GPS measurements. The oversized grab ring around the perimeter of the spar significantly simplifies deployment and recovery.

The hydrophone package (Fig. 1b) is a negatively buoyant shell with a hydrophone (HTI 99-UHF) at the base. The hydrophone package incorporates the same metadata sensors as the surface expression, as well as a pressure sensor (Blue Robotics BAR02 MS5837-02BA module, 5 Hz) to track depth. Hydrophone signals are captured by a custom circuit board with an analog-to-digital converter (Texas Instruments ADS127L01, up to 512 kHz) and high-precision oscillator (Abracon AST3TQ-T-16.384MHZ-28, 16.384 MHz $\pm$280 ppb). All sensors are tied into the same microcomputer architecture as the surface expression and data are saved to a solid-state memory card (64 GB). The lithium ion battery packs in the surface expression and hydrophone package (AA Portable Power Corp. CU-J610, 84 Wh) provide at least 24 hours of endurance, which exceeds the available storage capacity for hydrophone data under continuous recording at the maximum sample rate. The software integration of all sensors allows certain helpful functionality, such as disabling diagnostic WiFi when submerged (which would otherwise produce electromagnetic interference) and saving acoustic data only when submerged (which extends system endurance and reduces offload time). The hydrophone is elastically connected to a PVC guard. The electronics housing (Blue Robotics, 10.2 cm inner x 19.8 cm length) is contained within a

PVC pipe and incorporates closed cell foam at the top and lead sheet at the base to generate a righting moment. Without this, tether tension from the surface expression produces a continuous tilt in currents.

2.2 Operations Concept

Given the in-air weight of the surface expression (12 kg) and hydrophone package (6 kg), multiple DAISYs can be easily deployed from a small vessel (> 4 m length) by a crew of two. Most DAISY operations to date have been performed from vessels with relatively low freeboard (e.g., rigid inflatables), which provide favorable working conditions for deployment and recovery. Once DAISYs are deployed, the vessel moves off to a distance and powers down its engines and systems to minimize its own radiated noise, we wait for the dominant waves, currents, and wind to transport the deployed DAISYs through the survey area, and then power the vessel back up for recovery. DAISY position is monitored throughout the drift using radio-frequency trackers (Garmin T5 mini hunting dog collars) and associated handheld unit (Garmin Astro). While we incorporated a radio-frequency link into the surface expression, we found the range to be unacceptably limited to a few hundred meters due to the frequency limitations for unlicensed portions of the radio spectrum (900 MHz and 2.4 GHz) and low antenna elevation relative to the surface. At closer range, recovery is facilitated by reflective flags (Fig. 1a) and flashing white lights on the mast below the meteorological station.

2.3 Acoustic Performance

2.3.1 Calibration

Hydrophones were calibrated in multiple facilities: bench top low-frequency (1-700 Hz) by Ocean Networks Canada (ONC) (Biffard et al., 2022), in-situ mid-frequency (2-100 kHz) by ONC, and high-frequency (50-200 kHz) in a tank by Pacific Northwest

National Laboratory (PNNL). Additional details are provided as Supplemental Information. Above 40 Hz, the receive voltage sensitivity for the system is relatively stable at approximately -175 dB re 1 V/μPa. For the overlapping region of high-frequency calibration (50-100 kHz), we use the ONC calibration below 70 kHz and the PNNL calibration above. The differences between the reported sensitivities in this overlapping region are up to 5 dB, which is only partially explained by variations in azimuthal sensitivity (up to 2 dB at 50 kHz). This highlights challenges with calibrations across multiple facilities and implicit uncertainty in absolute measurements. We have routinely observed that pistonphone field calibration at 250 Hz (G.R.A.S. 42AA) is within 1 dB of the ONC calibration.

2.3.2 Acoustic Processing

Time-series of hydrophone voltage are split into 1-second windows (512,000 points) with 50% overlap. These are tapered using a Hann window and processed in MATLAB (Mathworks, R2023b) using the frequency-dependent calibrations to generate pressure spectral densities (PSD) with 1 Hz resolution. To reduce data volumes, variable band merging is used to calculate hybrid milli-decade levels (Martin et al., 2021; Bruce Martin et al., 2021), which have 1 Hz resolution below 435 Hz and lower resolution corresponding to 1/1000$^{\text{th}}$ of a decade at higher frequencies. PSDs are geo-referenced on the basis of their time stamps using linearly-interpolated surface expression GPS (x,y) and pressure logger (z) data. All metadata streams are packaged with the processed acoustic data.

2.3.3 Baseline Performance

To evaluate baseline system performance in the absence of significant wave or current forcing, we deployed a DAISY in the interior of Sequim Bay (WA) and compared received levels with a commercial hydrophone reference (Ocean Sonics icListen HF Reson) at the same depth. This location has relatively low ambient noise and, owing to light winds during this deployment, average speed over ground was ~12 cm/s. As shown in Fig. 2, the DAISY has similar performance to the reference hydrophone at frequencies up to 1 kHz. Beyond this, we reach the DAISY noise floor, evident in the collapse of the PSD probability distribution. While the DAISY noise floor is 10-15 dB higher than the commercial reference, this sensitivity is still sufficient to identify relatively high intensity radiated noise from marine energy converters and satisfies IEC specifications(IEC, 2019). We note that initial DAISY development used a similar hydrophone to the reference (Ocean Sonics icListen HF) due to ease of use and sensitivity, but, ultimately this limited the degree of possible customization.

3 Performance in Currents

To minimize flow noise in currents, it is necessary to minimize the relative velocity between the hydrophone and surrounding water, since this will result in turbulent eddies being shed by the hydrophone and expose the hydrophone to turbulence advected by the mean current. As demonstrated in Section 3.2, if there is limited vertical shear and coherent turbulence in the water column, flow noise can be minimized by simply suspending a hydrophone from a surface drifter, as in Lossent et al. (2018). However, because this does not guarantee flow noise minimization, a more robust approach is to surround the hydrophone with a "flow shield". The DAISY flow shield design was inspired by the fabric drogue used for "Drifting Ears" (Wilson et al., 2014) and uses a fabric (84% polyester and 16% spandex, "DriFit Wicking Spandex Ripstop", Seattle Fabrics) with high durability that rapidly shed air bubbles from its surface when submerged. The latter property is associated with the fabric structure: a hydrophobic layer sandwiched between two hydrophilic layers. As shown in Fig. 3, this fabric forms an oblong fabric shell with the hydrophone positioned roughly at the center. The shell is given form by three tensioned metal rods (4.1 mm spring-tempered stainless steel) tied into a clamping collar. The final design works well, but required

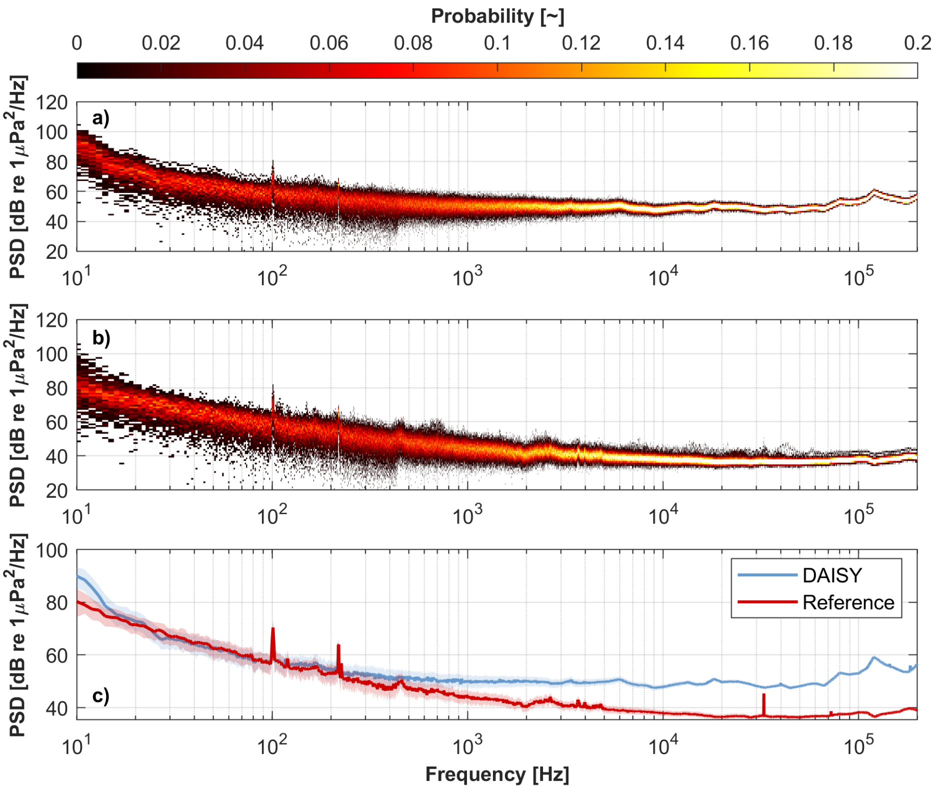

Fig. 2 Baseline acoustic performance during quiescent conditions in Sequim Bay, WA. (a) DAISY PSD probability distribution, (b) Reference hydrophone (icListen HF Reson) PSD probability distribution, and (c) Inter-comparison of median (solid line) and inter-quartile range (shaded region). The shared tonal peaks at 100 and 218 Hz are associated with ambient noise. The transition to millidecade processing causes the statistical contraction at 435 Hz.

repeated iteration from the initial approach of graphite kite spars in place of metal rods and a lighter weight clamp for the metal rods–both of which proved insufficiently durable for repeated deployment and recovery.

The shield suppresses flow noise in two ways. First, because of its size, it is a more significant source of drag than the surface expression. Consequently, the shield generally moves with the mean currents and pulls the surface expression with it when there is appreciable vertical shear between the two elements. Second, the shield attenuates turbulent eddies advected by the mean flow. The shield is connected to the surface

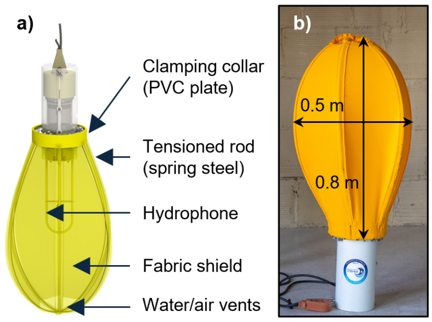

Fig. 3 (a) Annotated rendering of flow shield and (b) as-built shield with major dimensions.

expression by a variable-length tether. To date, we have used a solid rubber cord (9.53 mm EPDM rubber), terminated at each end with a plastic thimble embedded in a thick, cast urethane coating. This makes the tether easy to handle on deck and eliminates self-noise at the connection points. While some tether compliance is beneficial, system performance in currents does not appear to be particularly sensitive to tether composition (Appendix B).

The remainder of this section quantifies flow shield performance. Prior to this, we wish to remark on three poor-performance approaches that we tested during design iteration. First, we evaluated an in-line drag element proximate to the hydrophone (Pacific Gyre Microstar) in place of a flow shield, but found this difficult to deploy and recover. In addition, in downwelling currents, we discovered that the drogue generated sufficient force to entirely submerge the surface expression. In contrast, drag from downwelling currents causes the flow shield to contract and elongate, shedding load. Second, we tested an open cell foam annulus, which would be significantly more compact and has proved effective in another study with stationary a hydrophone (Lee et al., 2011). While this did reduce flow noise, we observed attenuation of propagating sound by > 20 dB above 1 kHz, which we hypothesize to be related to air bubbles retained in the foam (even when pre-treated with surfactant). Similarly, using a plastic shell as a flow shield did not appreciably reduce flow noise and attenuated propagating sound by > 10 dB from 4-20 kHz. This is not to say that other flow shield designs might not be as effective as the one adopted here. For example, Cotter et al. (2024) recently demonstrated the ability of oil-filled and ballistic nylon flow shields to substantially reduce flow noise for a stationary hydrophone in energetic currents. Appendix A focuses on the potential for the fabric flow shield to distort measured sound and the limited circumstances under which this may occur.

3.1 Methods

DAISY performance in currents was benchmarked in three ways.

First, to quantify flow noise reduction relative to a stationary hydrophone, a DAISY equipped with a flow shield was drifted over a hydrophone (Ocean Sonics icListen HF) deployed near the seabed in the entrance channel to Sequim Bay (WA). During this test, the DAISY tether was 2.5 m in length, placing the drifting hydrophone at a depth of 3.9 m. The stationary hydrophone was integrated into an Adaptable Monitoring Package (AMP) (Polagye et al., 2020). Due to a miscommunication about the AMP data acquisition cycle during this experiment, acoustic data were only collected for one minute at the top of each hour, so measurements were co-spatial, but not fully co-temporal. During this test, the DAISY drift rate, roughly equivalent to the mean current speed, was 0.98 ± 0.04 m/s and wind speed was 7.9 ± 0.9 m/s. Comparisons between the DAISY and stationary hydrophone were made for horizontal separation ≤ 15 m. These measurements are compared to the unshielded hydrophone deployed in a similar location by Cotter et al. (2024) for the same band of current speeds.

Second, to quantify the reduction in relative velocity afforded by the flow shield, a pair of DAISYs were modified to incorporate acoustic Doppler velocimeters (ADVs, Nortek Vector) sampling at 32 Hz in place of their hydrophone packages. One DAISY was equipped with a flow shield, the other was not equipped with a flow shield, but did have a drogue (Pacific Gyre Microstar) in line above the ADV. No motion correction was performed on the ADV data under the assumption that their motion would be similar to a hydrophone element and, consequently, characterize physically-relevant velocities. ADV data were despiked using the method of Goring and Nikora (2002). This test was also conducted in the entrance channel to Sequim Bay in mean currents of ∼1.6 m/s.

Finally, to assess the relative benefits of a flow shield in more realistic conditions, three DAISY variants with longer tethers (5, 10, and 15 m) were deployed in Admiralty Inlet (WA), a relatively wide (5 km) and deep (60 m) channel at the entrance to Puget Sound. During these tests, current speeds exceeded 3 m/s and winds were light at ∼2 m/s. The drifting hydrophone variants consisted of:

- a DAISY equipped with a flow shield;
- a DAISY without a flow shield; and
- a reference hydrophone (Ocean Sonics icListen HF Reson) without a flow shield suspended from a DAISY surface expression. Metadata for this hydrophone was provided by an autonomous 6-DOF IMU (Lowell Instruments MAT-1 logger) and pressure sensor (Onset HOBO). This configuration was more compact than the hydrophone package on a DAISY and representative of a low-complexity drifter.

A fourth DAISY without a flow shield was retrofitted with an ADV to characterize relative velocity for the unshielded hydrophones. However, unlike the prior test in Sequim Bay, a drogue was not included in-line with the ADV to minimize the potential for surface expression submersion. The data from this test was also used to evaluate potential attenuation of propagating sound by the flow shield (Appendix A).

To investigate the relationship between measured relative velocity fluctuations and flow noise, the theoretical pressure spectral density arising from flow noise was calculated from the ADV velocity spectra ($N = 256$ points, 80% window overlap, Hamming taper). Strasberg (1979) describes the theoretical pressure spectrum (S_{pp}) arising from relative velocity perturbations as

$$S_{pp}(f) = \rho^2 \langle U_o^2 \rangle S_{uu}(f) \tag{1}$$

where ρ is the seawater density (1025 kg/m^3), U_o^2 is the mean-square relative velocity, and $S_{uu}(f)$ is the velocity power spectrum. U_o^2 is calculated as the velocity-squared magnitude measured by the ADV during the drift (the left and right angles denote the mean value of the this quantity), and S_{uu} is assumed equal to the vertical velocity spectrum S_{ww}, which has a lower noise floor. This assumption is valid in the inertial subrange where turbulence is isotropic and follows an $f^{-5/3}$ dependence (Taylor, 1937). The theoretical pressure spectral density is then given as

$$PSD_{\text{theory}} = 10 \log_{10} \left(\frac{S_{pp}(f)}{p_{\text{ref}}^2} \right) \tag{2}$$

where the reference pressure, p_{ref}, is 1 μPa.

3.2 Results

Fig. 4 demonstrates that, relative to a stationary hydrophone, the DAISY suppresses flow noise at frequencies below 400 Hz. For a stationary hydrophone, flow noise exceeds ambient noise by more than 40 dB at 100 Hz and masks the prominent tone at 170 Hz associated with a nearby seawater intake pump. This masking occurs even though the stationary hydrophone is positioned in the channel boundary and likely exposed to lower flow velocities than the DAISY. Similarly, because flow noise intensity increases with current speed (Bassett et al., 2014; Cotter et al., 2024), the affected frequency range would be wider at current speeds relevant to tidal power generation. While the AMP measurements are not strictly co-temporal with the DAISY measurement, their similarity suggests a relatively stationary soundscape and are consistent with longer-term measurements by Cotter et al. (2024) at similar current speed.

Even drifting and equipped with a flow shield, at frequencies below 20 Hz, the DAISY experiences appreciable flow noise from residual relative velocity. At the same time, it is also important to contextualize this limitation relative to the lowest frequency sound that can propagate at a site based on the modal cut-off (Jensen et al., 2011). This can be approximated as

$$f_{\mathrm{low}} = \frac{c}{4D\left(1 - \frac{c^2}{c_s^2}\right)^{\frac{1}{2}}} \tag{3}$$

where D is the water depth, c is the speed of sound in water, and c_s is the speed of sound in the seabed. While none of these parameters are known exactly for the test conditions (D ∼8 m, c ∼1500 m/s, c_s ∼1700 m/s), they suggest a modal cut-off on the order of 100 Hz. This means that the presence of flow noise at frequencies below 20 Hz in drifting measurements is unlikely to meaningfully impair measurement of radiated noise from a current turbine at this location because sound generated at frequencies below the modal cut-off would decay rapidly. Locations with deeper water would have a lower cut-off frequency (e.g., on the order of 10 Hz for 60 m depth). However, even when it does propagate, sound at frequencies lower than 10 Hz is not of general interest for environmental monitoring around marine energy converters because of marine animal auditory thresholds (Hawkins et al., 2014; NMFS, 2018).

Turning to the relative velocity measurements, residual velocities inside the flow shield are, on average < 5 cm/s (Fig. 5b), while ambient relative velocities can be an order of magnitude higher (Fig. 5a). Notably, the unshielded ADV does, in some instances, encounter velocities as low as those inside the shield. This suggests that flow noise may be similarly intermittent, which is explored further in the measurements from Admiralty Inlet. Finally, considering the spectral density of vertical velocity (Fig. 5c), we see that the unshielded ADV measures the expected decay for isotropic turbulence (Taylor, 1937). This is likely also occurring for the shielded ADV, but is not readily observable before being masked by the instrument noise floor.

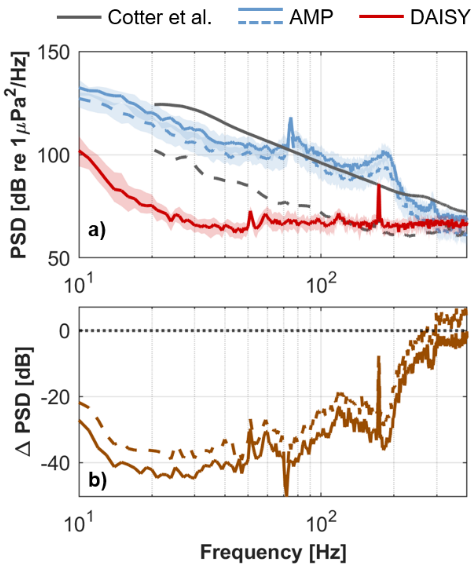

Fig. 4 (a) Comparison of received levels for a DAISY and stationary hydrophones in Sequim Bay entrance channel (WA). Cotter et al. (2024) for 0.8-1.0 m/s current speed, AMP measurements from 20 minutes prior to (solid line) and 40 minutes following (dashed line) the DAISY drift on a falling ebb tide. Lines denote medians and shaded regions denote interquartile ranges. (b) Received level variation between stationary AMP hydrophones and DAISY.

DAISY performance in Admiralty Inlet is summarized in Fig. 6. Here, we consider frequencies below animal hearing limits to make comparisons with theoretical estimates for flow noise based on co-temporal drifting ADV measurements. Beginning at the highest frequencies (10-100 kHz), we see clustering by tether length associated with temporal variability in ambient noise. Unlike the quiescent benchmark test in Sequim Bay (Fig. 2), we observe good agreement between the DAISYs and reference hydrophone because ambient noise exceeds the DAISY noise floor. This similarity extends to the majority of the mid-frequency range (0.1-10 kHz) with the exception of the 1-10 kHz range for the DAISY on a 10 m tether. Given the affected frequencies, we hypothesize that this deviation is caused by drifting through the bubble plume produced by the deployment vessel which causes upward refraction of propagating sound. From these measurements, we conclude that the flow shield does not materially

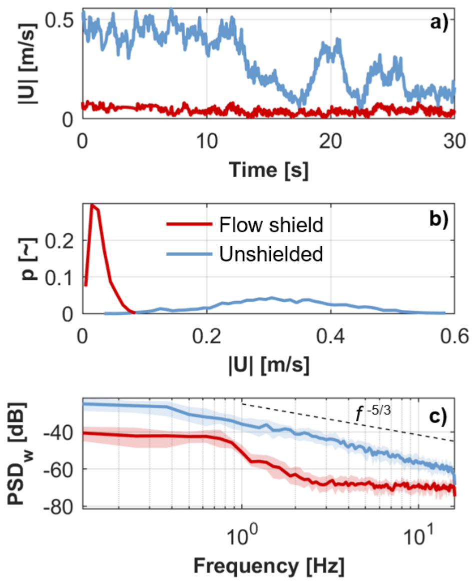

Fig. 5 (a) Representative time series comparison of velocity magnitude measured by ADV surrounded by flow shield and ADV exposed to ambient flow. (b) Probability distribution of velocity magnitude for the two configurations. (c) Velocity spectral density for the vertical component of measured velocity. The expected spectral decay with frequency from isotropic turbulence is indicated by the dashed black line.

distort propagating sound at any frequencies of interest for marine energy converters (Appendix A). We also note that the soundscape is consistent with prior passive acoustic studies in Admiralty Inlet. Above 10 kHz, this may be dominated by sediment-generated noise (e.g., cobble and pebble collisions) in agreement with Bassett et al. (2013). Similarly between 20 and 1000 Hz, where anthropogenic noise dominates at this location, measurements are in agreement with the low vessel traffic state reported in Bassett et al. (2012), matching visual evidence of vessels during the experiment.

Below 100 Hz, differences emerge across the variants. Overall, the DAISY equipped with a flow shield is least affected by flow noise, consistent with benchmark tests in weaker currents. Around 8 Hz, the shielded and unshielded DAISY have a self-noise peak that is likely caused by vibration of the hydrophone assembly (e.g., relatively long-stemmed hydrophone), excited by tether strum. This can be reduced by adding

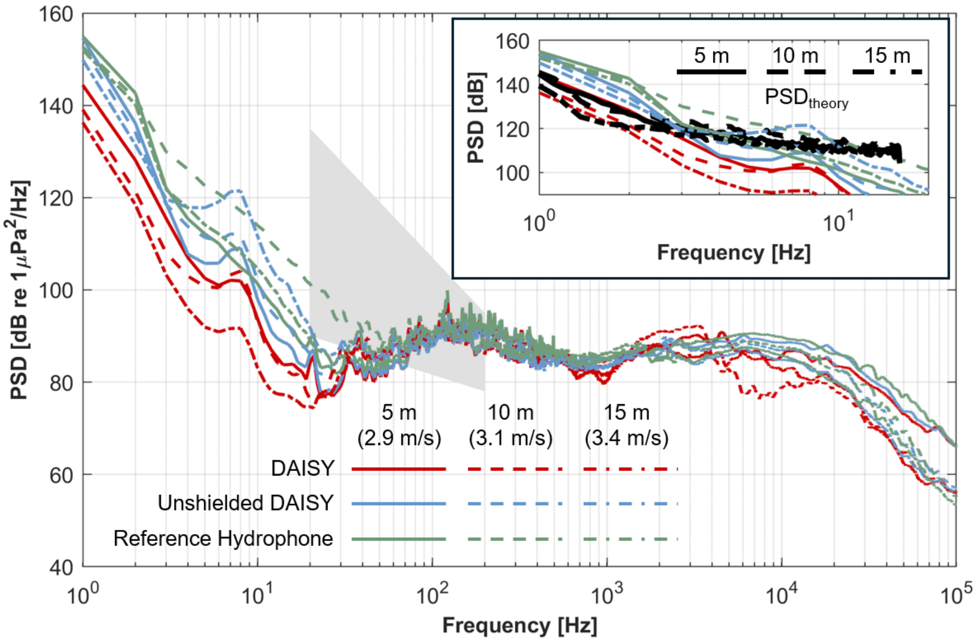

Fig. 6 Intercomparison of median PSDs between a DAISY and other drifting hydrophone variants in Admiralty Inlet (WA) with 5, 10, and 15 m tethers. Parenthetical speeds are the mean currents during drifts at each tether length. The grey shaded region represents the range observed for a stationary platform in this location during periods with similar near-surface currents (Bassett et al., 2014). (inset) Low-frequency (1-20 Hz) performance compared to theory for flow noise based on co-temporal drifting ADV measurements.

a fairing to the tether (Appendix B). The reference hydrophone has inconsistent performance, with more significant flow noise for a 10 m tether than for the 5 m or 15 m. Finally, we note that, in comparison to stationary measurements during periods with similar near-surface currents (Bassett et al., 2014), the DAISYs experience up to 40 dB less flow noise for received levels around 30 Hz.

Comparing measured flow noise to theoretical estimates (Fig. 6, inset), we observe good agreement with theory for the DAISY with a flow shield for frequencies up to 2 Hz. At higher frequencies, the divergence between theory and observation is caused by two factors. First, the turbulent spectrum should decay at a constant rate in the inertial subrange until reaching the Komolgorov scale where turbulent motion is entirely dissipated as heat (Taylor, 1937). The divergence of the theoretical spectrum from a constant slope is caused by Doppler noise in the velocity measurement (Thomson et al., 2012). Second, even if the velocity measurement was noiseless, one would expect to eventually see observed flow noise decay faster than predicted by the velocity spectra. This is because, as frequency increases, the associated length scale for the turbulence falls below the size of the hydrophone and the pressure contributions from turbulent eddies begin to average out across the pressure-sensitive element (Strasberg, 1979). Given the observed relative velocity during the tests (0.1-0.4 m/s, independent of tether length), this averaging would be expected to be appreciable for frequencies higher than 10 Hz. This decay is not observed in the data, however, likely because propagating ambient noise begins to exceed flow noise at similar frequencies.

Interestingly, for the lowest frequencies, the theoretical spectra more closely tracks the residual flow noise inside the shield than experienced by the unshielded hydrophones. At first, this appears contradictory, given that the turbulence inside the flow shield is likely less energetic than in the surrounding water (Fig. 5). However, flow noise arises from two mechanisms: (1) the advection of turbulence over the hydrophone element and (2) turbulence from shed vortices arising from relative velocity between the hydrophone and surrounding water. The first mechanism is described by Eq. 1, but the second is not and both mechanisms are likely present for the shielded and unshielded hydrophones. For the shielded hydrophone, it is plausible that Eq. 1 is over-predicting the contribution from advected turbulence inside the shield, but this is roughly equivalent to flow noise caused by eddy shedding. For the unshielded hydrophones, relative velocity is likely substantially higher (Fig. 5), such that the observed flow noise is higher amplitude than predicted by theory.

Returning to the overall performance, we do not see a consistent and interpretable relationship between flow noise and tether length. Going into these tests, we had hypothesized that relative velocities and, consequently, flow noise would increase with tether length due to greater vertical shear between the hydrophone packages and surface expressions. However, at frequencies around 10 Hz, the shielded and unshielded hydrophones experienced similar flow noise during some tests. Understanding the reasons for this requires a consideration of the time series that underlie the median PSDs.

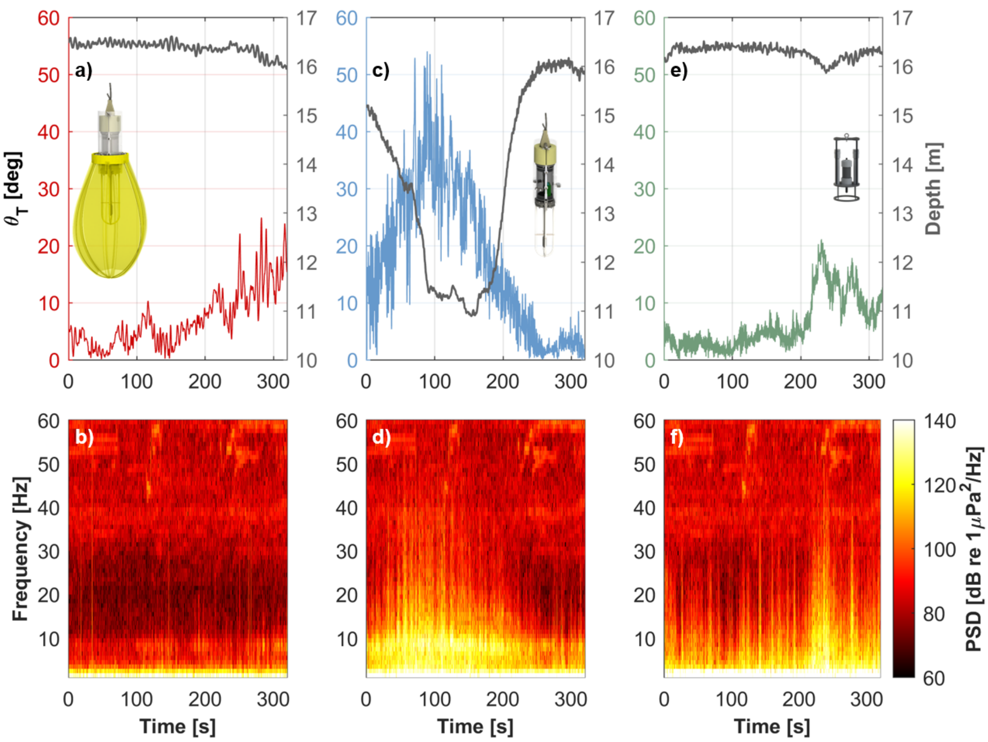

Fig. 7 Time series of hydrophone package tilt and hydrophone depth for (a) DAISY, (c) DAISY without flow shield, and (e) reference hydrophone with 15 m tethers. Tilt coloration matches drifter configuration in Fig. 6. Hydrophone depth is greater than the tether length due to the vertical extent of the surface expression and hydrophone package. (b,d,f) Low-frequency (0-60 Hz) spectrograms for the same. Persistent tether strum at 8 Hz is apparent for the shielded and unshielded DAISYs.

Fig. 7 shows time series information about hydrophone package orientation and associated low-frequency (0-60 Hz) spectrograms for drifts with 15 m tethers.

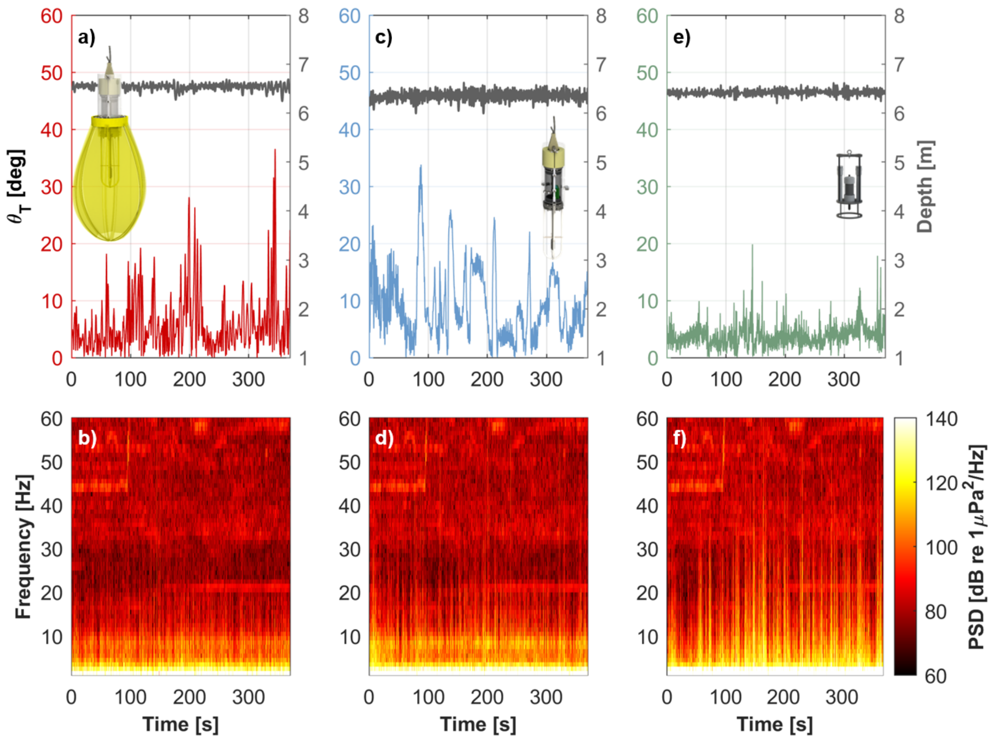

Fig. 8 As for Fig. 7, but with a 5 m tether

Hydrophone package tilt is defined as

$$\theta_T(t) = \cos^{-1}(\sqrt{1 - \sin^2 \theta_R(t) - \sin^2 \theta_P(t)}), \tag{4}$$

where $\theta_P(t)$ is the time-varying pitch angle and $\theta_R(t)$ is the corresponding roll angle measured by the IMUs. The unshielded DAISY (Fig. 7c,d) experiences a significant excursion in tilt and depth during a portion of the drift, likely forcing from a coherent turbulent structure. During this time, flow noise is correspondingly elevated. The reference hydrophone does not experience a depth excursion, but, near the end of the drift, flow noise is elevated when there is a persistent tilt. We interpret this as an indication of relative velocity on the hydrophone package due to tension from the surface expression. In contrast, when similar persistent tilt occurs for the DAISY equipped with a flow shield, no flow noise is generated. While the maximum flow noise intensity is similar for the two unshielded hydrophones, the median PSD associated with flow noise (Fig. 6) is lower for the reference hydrophone because the flow noise is more intermittent. The inversion of the median PSDs for these configurations with a 10 m tether is a consequence of relative variations in hydrophone package tilt and depth that affect flow noise intermittency (see Supplementary Information). This suggests that the extent to which flow noise affects an unshielded, drifting hydrophone is a matter of circumstance. For example, during the drifts with 5 m tethers, hydrophone package motion was too limited to produce substantial flow noise for either unshielded hydrophones (Fig. 8). As such, the median PSDs at frequencies $<$ 20 Hz are similar for all three variants (Fig. 6).

In summary, for an unshielded drifting hydrophone, there are two mechanisms that likely increase relative velocity and associated flow noise. The first is forcing by a coherent structure, which manifests as a depth and orientation change for the hydrophone package. The second is vertical shear between the surface expression and hydrophone, which manifests primarily as a sustained hydrophone tilt at near-constant depth. This can occur when the surface expression is the dominant source of drag and vertical shear is appreciable. Consequently, this mechanism is more likely to occur for deeper hydrophone packages.

While effective at suppressing flow noise, the flow shield is more cumbersome to deploy/recover and, because of drag on the flow shield, the hydrophone package takes longer to reach a steady-state depth. These results suggest that forgoing a flow shield is a viable strategy if a potentially lower data yield is acceptable. This does, however, require metadata about the hydrophone package orientation to exclude periods of time when flow noise is likely to mask propagating sound. Finally, since the shielded and unshielded hydrophone measurements converged above 40 Hz for these test conditions, shielding is likely more important at sites with a relatively low modal propagation cut-off (Eq. 3).

4 Performance in Waves

As in currents, minimizing flow noise in waves requires minimizing relative velocity between the hydrophone and surrounding water. Here, relative velocity can be produced by two sources: wave orbital velocities that decay exponentially with depth (Demirbilek and Vincent, 2002) and acceleration from tether tension when the surface expression is forced by waves. As for a sonobuoy, the hydrophone package can be isolated from surface expression motion by incorporating a "heave plate" into the tether connection (Fig. 9). When accelerated in the vertical direction, heave plates generate added mass from the proximate acceleration of water (Stokes, 1851) that can be an order of magnitude higher than the static mass of the plate. In combination with an elastic tether, this results in a mass-spring-damper system that minimizes tether tension on a hydrophone package at depth. Compared to the flow shield used in currents, the heave plate construction for the DAISY is relatively simple–most components are off-the-shelf PVC fittings for plumbing applications. Because metallic shackles are used to connect the heave plate and tether, the heave plate connection points are potted in urethane to minimize self-noise.

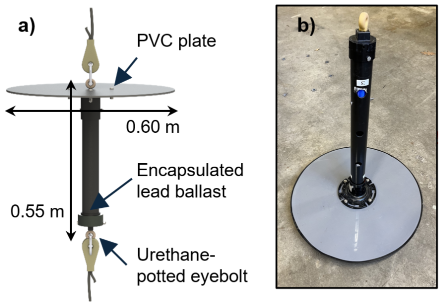

Fig. 9 (a) Annotated rendering of heave plate with major dimension and (b) as-built heave plate. When deployed, the heave plate orientation is as shown in the rendering.

4.1 Methods

DAISY performance in waves was benchmarked at the U.S. Navy's Wave Energy Test Site (WETS) in Kaneohe, HI. Three drifting hydrophone variants were evaluated:

- a DAISY with a tether system (starting from the surface expression) consisting of a 7 m rubber cord (9.53 mm EDPM rubber), heave plate assembly (Fig. 9), and 2.5 m rubber cord ("heave plate" configuration);
- a DAISY with the same tether lengths, but without a heave plate and with a flow shield installed on the hydrophone package ("flow shield" configuration); and
- a DAISY with the same tether lengths, but neither heave plate nor flow shield ("rubber only" configuration).

Because of the different elements present in each tether, as well as tether-to-tether manufacturing variability, hydrophone depth varied for the three systems: 13.4 m for the variant with a heave plate, 11.4 m for the variant with a flow shield, and 10.9 m for the variant with only rubber. The sea state during this test was measured by a moored buoy (Datawell Wave Rider, CDIP Station 198), which reported a significant wave height of 1.8 m and energy period of 6.8 s. Wind speed was $\sim$4.5 m/s and water depth was $\sim$75 m. The data from a similar test was also used to evaluate the potential attenuation of propagating sound by the flow shield (Appendix A).

4.2 Results

Performance of the three variants is shown in Fig. 10. The DAISYs equipped with a heave plate and with a flow shield have nearly identical performance at frequencies above 15 Hz. Below this, the DAISY equipped with the flow shield experiences slightly more flow noise than the one with the heave plate. When no drag or inertial elements are included in the tether, performance is quite poor, with flow noise masking ambient noise to at least 100 Hz.

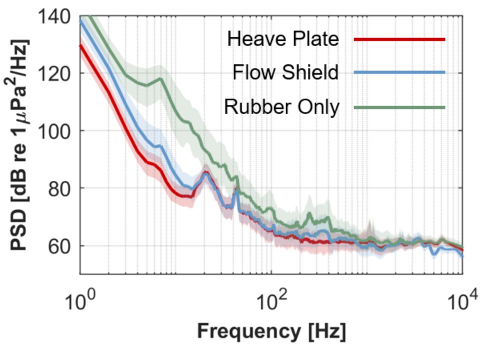

Fig. 10 Intercomparison of median PSDs between DAISYs equipped with a heave plate, flow shield, and neither (rubber tether only) at WETS (HI). Solid lines denote median PSDs and shaded regions are the interquartile range.

The reason for these differences is apparent in the relative motion of the hydrophone package (Fig. 11). When only a rubber tether is used in line between the surface expression and hydrophone package, surface expression motion is appreciably translated to the hydrophone, leading to significant motion (Fig. 11g,h), relative velocity, and flow-noise (Fig. 11i). The DAISY equipped with the flow shield experiences more motion than the one equipped with the heave plate (Fig. 11d,e relative to Fig. 11a,b). This is likely because the heave plate generates substantially more inertia through added mass when it comes under tension through the tether. However, as for operation in strong currents that produce significant hydrophone package motion (e.g., Fig. 7), the largely quiescent volume within the flow shield minimizes flow noise. Given that the heave plate is easier to deploy/recover than the flow shield, this has remained our preference for field measurements in waves, but either approach is likely acceptable. If operating in substantial waves and currents, the flow shield, potentially in combination with a heave plate, could be preferable.

While IMU data was not available for the variant intercomparison, performance in a similar sea state (Fig. 12) demonstrates that the combination of the rubber tether and heave plate substantially isolates the hydrophone package from surface expression motion. We note that the choice of tether lengths employed (7 m between the surface

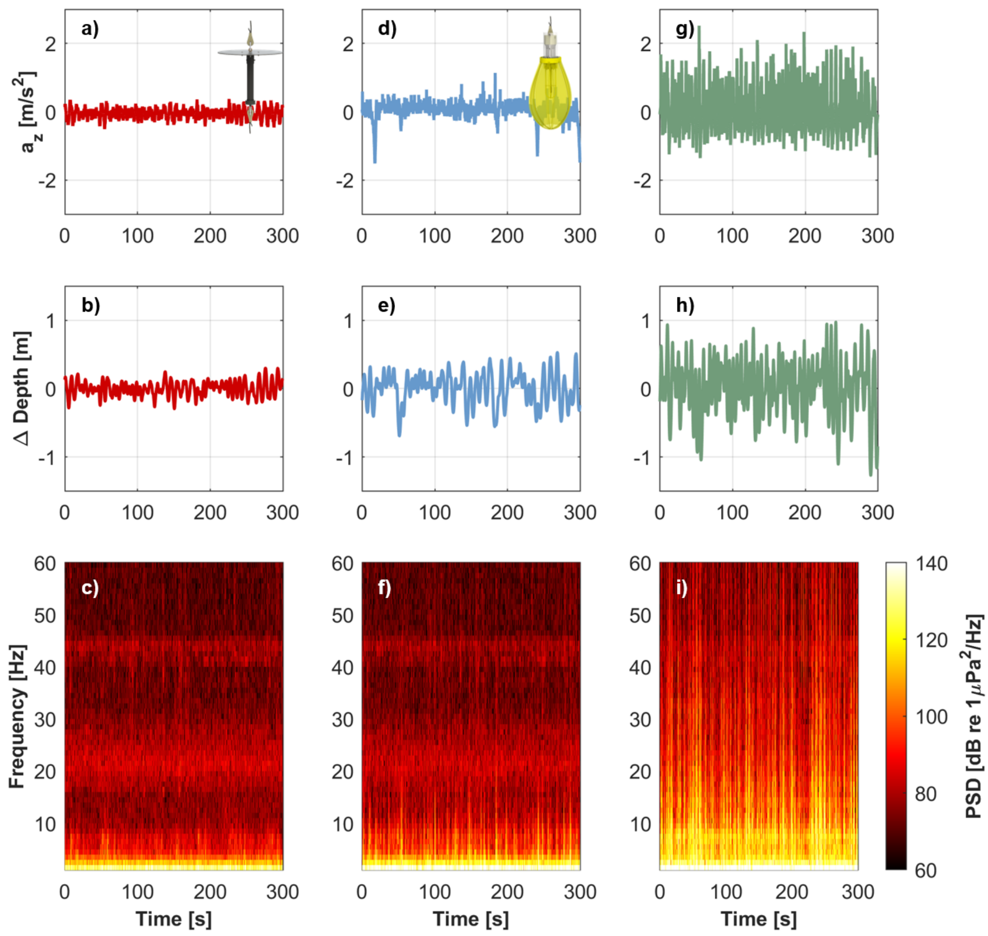

Fig. 11 Motion and associated flow noise for DAISYs equipped with a heave plate (a-c), flow shield (d-f), and neither (rubber tether only, g-i) at WETS (HI). (top row) Heave acceleration for the hydrophone package. Surface expression acceleration was not available due to intermittent IMU data logging during this test. (middle row) Change in depth relative to the average for the drift. (bottom row) Low-frequency (0-60 Hz) spectrograms.

expression and heave plate, 2.5 m between the heave plate and hydrophone package) was semi-arbitrary. We have performed other tests with a longer tether between the heave plate and hydrophone and found this to provide similarly effective motion isolation. Depending on the sea state, shortening the tether between surface expression and heave plate could eventually cause the hydrophone to experience problematic relative velocities. For the case presented here, for a linear wave with the same height

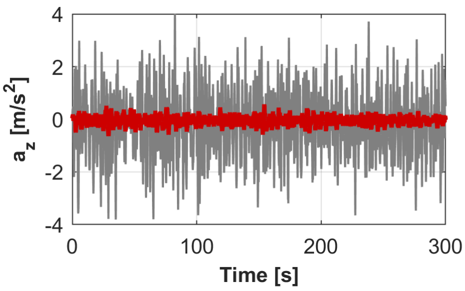

Fig. 12 Heave acceleration for surface expression (grey) and hydrophone package (red) for a DAISY equipped with a heave plate. During this test, the significant wave height was 1.8 m and the energy period was 7.6 s.

as the significant wave height (1.8 m) and same period as the energy period (7.6 s), the maximum orbital velocity at hydrophone package depth (∼12.7 m) would be ∼0.3 m/s (Demirbilek and Vincent, 2002). Because this is oscillatory with the wave period, on average, flow noise is quite limited, even though the hydrophone is unshielded. For more energetic waves or a shallower hydrophone, appreciable flow noise could extend to higher frequencies.

5 Localization

Since not all sounds are easily attributable to marine energy converters, localization capabilities can help disambiguate between sources of unknown origin. While localization can be performed with vector sensors that measure acoustic velocity (Raghukumar et al., 2020; Tenorio-Hallé et al., 2022), these have limited frequency bandwidth and, consequently, may not be able to localize all sounds of interest for marine energy converters (e.g., frequencies associated with power electronics excitation up to 10s of kHz). An alternative to vector sensors is time-delay-of-arrival (TDOA) using multiple hydrophones in a long baseline array (e.g., Watkins and Schevill (1972)). Accurate TDOA localization requires a sufficient signal-to-noise ratio to identify the signal time of arrival at each receiver, knowledge of receiver locations, and measurements of sound speed. Correspondingly, TDOA errors are driven by ambiguity in the time of arrival at each receiver, GPS uncertainty in receiver locations, displacement between the receiver and GPS antenna, unfavorable receiver geometry relative to the source, and uncertainty in the sound speed.

5.1 Methods

DAISY localization capabilities were evaluated at WETS (Section 4.1) with five DAISYs using the heave plate tether system described in Section 4. No WECs were present during these measurements, but WETS has fixed mooring infrastructure. At the berth in 60 m water depth, there are three surface buoys (4.2 m diameter) anchored to the seabed by mooring chains. The buoys form an equilateral triangle roughly 250 m on edge and, in the absence of a WEC, are tensioned together at a central connection point to limit mooring motion. However, before the test, one buoy had broken loose from the central connection, was experiencing greater motion, and, consequently, likely producing more noise. Over an hour-long period, DAISYs were deployed in drifts bracketing all three buoys at the berth or only the unrestrained buoy. The majority of these drifts used the same tether length for all DAISYs, resulting in a planar array. For one set of drifts around the unrestrained buoy, the performance of a non-planar array was evaluated by lengthening the tether on two DAISYs to increase the hydrophone depth from $\sim$12 m to $\sim$18 and $\sim$22 m. During these test, the significant wave height was $\sim$1.9 m, energy period was $\sim$7.4 s and wind speed was $\sim$6 m/s.

Recordings contained multiple metallic rattling noises, likely from chain contact between mooring components as the buoys heaved. For the first and last 60 s of each drift, all signals of interest were manually identified through visual review of one receiver's spectrogram and an approximate time and frequency range was recorded for each event. These times were then refined by reviewing the associated voltage waveforms. Event duration ranged from a fraction of a second to several seconds, with the most intense sounds between 700 and 3500 Hz. For each event, detrended hydrophone voltage was bandpass filtered over this frequency range. The $n+1$ signals with the highest signal-to-noise ratio were retained for TDOA processing, where n is the dimensionality of solution (e.g., 2D, 3D) . Cross-correlation to identify arrival times was performed on Hilbert-transformed signals (Buaka Muanke and Niezrecki, 2007), using the highest signal-to-noise ratio event as the matched filter. We note that the Hilbert transform significantly increased the correlation coefficients during this step in the process. Fig. 13 shows an example of this pipeline for a representative 2D localization.

Once the time of arrival is established, this information is combined with the DAISY locations to estimate the source position using TDOA. In a well-mixed environment (which is the case at WETS due to near-constant wave action, see Supplementary Information), the sound travel time is directly proportional to the distance between the source and receiver. The difference in arrival times at each set of two receivers defines a hyperbola of possible source locations. Three receivers define two hyperbolas, with the two-dimensional source location at their intersection. Four receivers locate a source in three dimensions. Here, the solution method described by Wahlberg et al. (2001) is used to estimate 2D or 3D source position. To evaluate the potential benefit of including additional receivers, a least-squares solution is also considered for 2D source position. While, for this example, the least-squares solution always returns a single solution, the exactly determined solutions in 2D and 3D can generate two estimates for source location. For 3D, choosing the correct solution is trivial, as only one position is located below the water surface. For 2D, we determined that the smaller of the two real roots is most often correct.

5.2 Results

Source localization (Fig. 14) places the vast majority of the acoustic events ∼20 m west of the nominal location of the unrestrained buoy. Depending on the specific localization

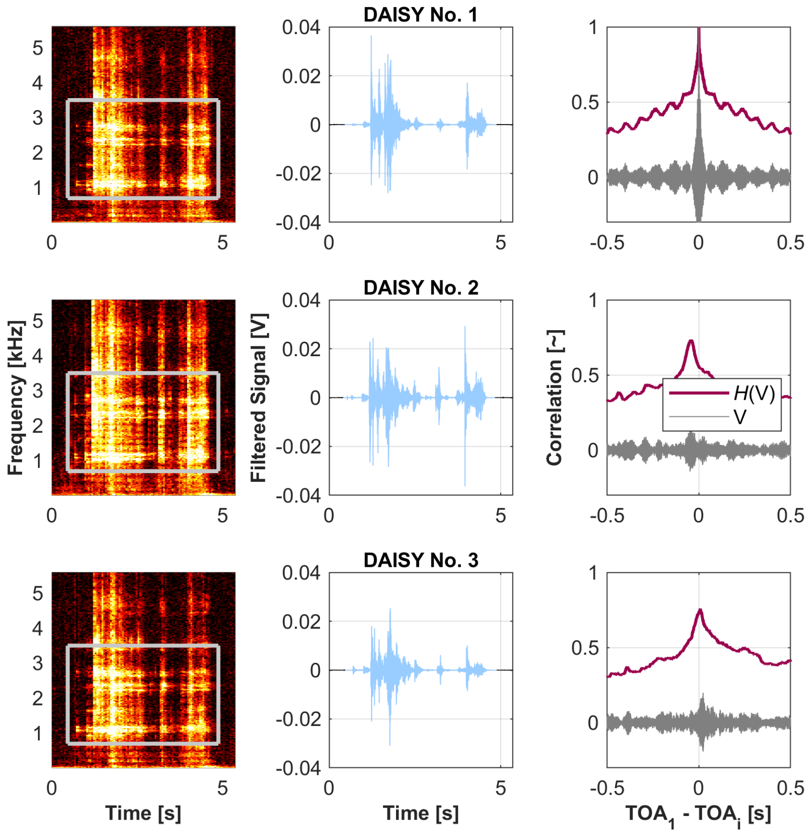

Fig. 13 Representative example of 2D localization of a mooring noise event for three DAISYs in order of decreasing signal-to-noise ratio. (left) Spectrogram (color ranges from 60-100 dB re $1\mu Pa^2$/Hz with bright colors denoting more intense sound. (middle) Filtered voltage (black) with event identified by cross-correlation (blue). (right) Correlation coefficient as a function of lag time for filtered voltage and Hilbert-transformed voltage, $H(\mathrm{V})$.

scheme, a limited number of events are also localized to the other two buoys and the differences in received levels are consistent with those position estimates. The fraction of events originating from the unrestrained buoy is consistent with the hypothesis that its additional motion would produce noise more frequently. The median position estimates for the source of noise from the unrestrained buoy were similar for all deployment configurations (within 10 m radius, colored squares in Fig. 14d-f). The variability in estimated source position could reflect mooring movement, but are more likely a consequence of localization uncertainty. Specifically, comparing the exactly (Fig. 14a,d) and overdetermined (Fig. 14b,e) estimates, we see that the overdetermined estimates have less variability. This is consistent with expectations for an overdetermined solution, but in a limited number of cases, the overdetermined solutions lies farther from the median position. We hypothesize that this occurs when one or both of the additional receivers have relatively low signal-to-noise ratios, substantially increasing ambiguity in the signal time of arrival. While the 3D localization has less apparent scatter than either of the 2D solutions, this is an artifact of fewer events with a physical solution ($N = 57$ vs. $N = 79$ for the exact and overdetermined 2D solutions).

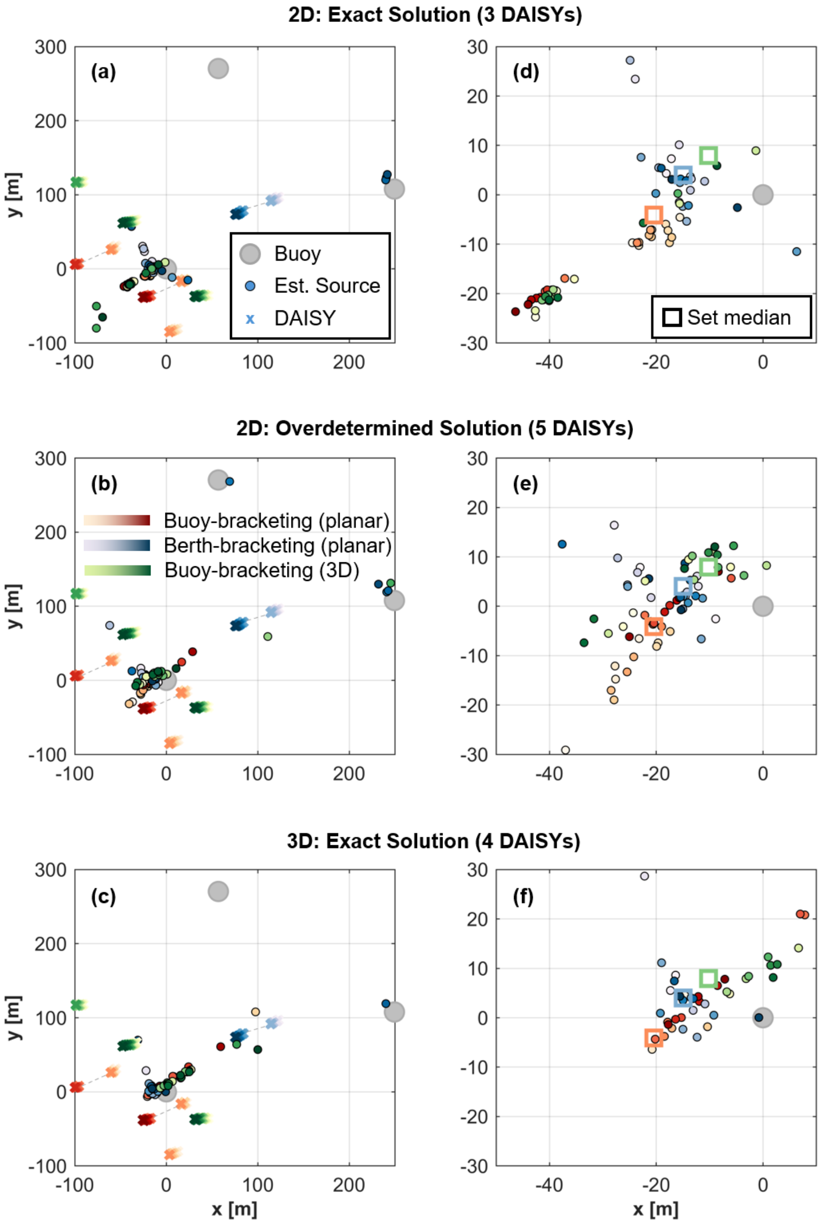

Fig. 14 2D (exact and overdetermined) and 3D localization of mooring noise. (left) Area view of the entire berth. (right) Detail view of the area around the unrestrained buoy. Colors denote the general DAISY release configuration and thin, dashed grey lines connect the same DAISY unit within a given release configuration. Some DAISY locations lie outside the axes limits. The buoy locations are nominal (as measured during installation) and the buoy markers are not to scale.

Estimated source depth from 3D localization (Fig. 15) suggests the sound produced by the unrestrained buoy is originating from near the seabed, which is consistent with the mooring construction. Source estimates, particularly for the berth-bracketing drift with an array of receivers at variable depth, are often beneath the seabed, though the median estimates from both planar arrays are similar to the actual water depth. We caution about drawing conclusions about a lack of benefit from staggered receiver depth. For this deployment configuration, one receiver was substantially further from the source than the others (and, therefore, excluded from the exactly determined solution on the basis of signal-to-noise ratio), while two of the remaining four receivers were in an unfavorable "end fire" configuration in line with the source. Consequently, the differences in estimated source depth for the non-planar and co-planar receiver arrays may be attributable to receiver orientation, rather than the vertical staggering.

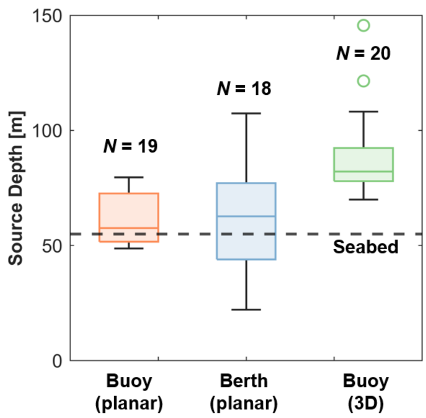

Fig. 15 Box plot representation of source depth estimates from 3D localization for events localized to the unrestrained buoy. Dashed horizontal line denotes seabed depth relative to surface (0 m).

As previously mentioned, errors in TDOA localization are caused by ambiguity in signal arrival times, uncertainty in receiver location, and unfavorable receiver geometry relative to the source. While time quantization and sound speed uncertainty can contribute to arrival time errors (e.g., Ehrenberg and Steig (2002)), these are likely subordinate to other sources of error. The DAISY GPS likely introduces an uncertainty of

$\sim$2 m into the position of each receiver, which is compounded by horizontal displacement between the GPS and hydrophone due to the tether between them. However, this is not likely appreciable relative to errors associated with arrival time ambiguity or receiver geometry. For example, given the measured sound speed of 1538 m/s (see Supplementary Information), an arrival time uncertainty of only $\sim$1.3 ms would be equivalent to a 2 m error in receiver position. For distributed instruments like a DAISY array, clock drift between receivers can be a concern. In design, this was addressed by obtaining pulse-per-second (PPS) synchronization with GPS while on the surface and employing a high-precision crystal oscillator (AST3TQ-28, Abracon LLC). While some clock drift does occur ($<$ 1 ms/hr), this should have limited impacts because DAISY deployments are $<$ 30 minutes in duration. An alternative design would be an electrical connection between the surface expression and hydrophone package, but this would be more costly (particularly for multiple tether lengths), the desired mass-spring-damper characteristics for flow noise suppression in waves would be more difficult to achieve (Section 4), and this would pose a greater risk of electromagnetic interference for the hydrophone ADC.

Array layout affects the accuracy of localization estimates through both the geometry of the receiver array and the distance between the receivers and the source. This method of localization is most accurate when the source is at the center of an equally-spaced, radially symmetric array which maximizes the region with a unique solution to the hyperbola intersection (Compagnoni et al., 2014). Additionally, in cases where the source is vertically displaced from the receivers, the error from neglecting that difference in depth for 2D localization is minimized for a source at the center of the array (Konagaya, 1982). If the source is outside the receiver plane, the closer the receivers are to the source, the proportionally greater the 3D slant distance (reflected in the signal travel time) will be compared to the 2D distance (reflected in the GPS positions). As the distance between the receivers and source increases, the slant distance error proportionally decreases, but the signal-to-noise ratio for signals of interest also decreases, making arrival times potentially more ambiguous. Given that the vertical distance between the DAISYs and source (∼40 m) is an appreciable fraction of the horizontal separation for the buoy-bracketing drifts, this may contribute to some of the scatter in the estimated horizontal positions for 2D localization. In addition, the distance between source and receiver can exacerbate other sources of uncertainty. As the distance increases, the hyperbolas of possible source locations intersect at increasingly small angles (Watkins and Schevill, 1972). Any ambiguity in arrival time will then cause a larger change in the location of the intersection point and therefore, the estimated source location.

The acceptable uncertainty in this application has some simplifying differences from bio-acoustics (Watkins and Schevill, 1972; Spiesberger and Fristrup, 1990; Macaulay et al., 2017). First, the source locations of interest are relatively well constrained by prior knowledge about infrastructure layout at a site. In this example, sounds of interest likely originated from three buoys, such that useful localization only requires that the uncertainty (i.e., spread in the source estimates) is smaller than the distance between candidate sources. Similarly, if all infrastructure is either located at the surface (e.g., a WEC) or seabed (e.g., moorings and anchors), then useful depth localization only needs to differentiate between the two limiting cases. Second, from the standpoints of environmental impacts or condition health monitoring, only sounds that frequently occur are of operational interest. As a result, not every instance of a signal needs to be successfully localized. Third, while infrastructure position can vary in time for compliant moorings, this is, again, relatively constrained, such that the median position from multiple localizations is more important than an individual realization.

In this example, we localized a sound with relatively high signal-to-noise ratio. Other sounds from WECs and current turbines that is lower intensity, but has a time-varying structure, such as sounds associated the power take-off or wave-float interactions, should be addressable within this framework. However, sounds with a near-constant tonal structure (e.g., power electronics excitation of generator windings) would likely require a different approach. Finally, we note that there are several approaches that could improve localization accuracy. First, the receivers included in an exact solution could be chosen on a basis other than signal-to-noise ratio (e.g., consideration of receiver geometry). Second, a minimum likelihood estimator (Macaulay et al., 2017) could be used instead of a solution to the hyperbolic equations (Abadi et al., 2019). Third, sound intensity variations across the receiver array could provide useful information about the source location (Cato, 1998). While more data, particularly from operating WECs or turbines is required, these preliminary results suggest that localization with arrays of DAISYs could be effective at identifying sound sources at marine energy sites and that an overdetermined number of receivers marginally increases accuracy relative to an exactly determined array.

6 Discussion & Conclusions

As demonstrated through these tests, Drifting Acoustic Instrumentation SYstems (DAISYs) can accurately measure radiated noise in energetic currents and waves. This type of capability should help to expand our understanding of radiated noise from marine energy converters. In currents, a flow shield is shown to effectively suppress flow noise, even when mean currents exceed 3 m/s. Similarly, in waves, a tether incorporating a heave plate effectively isolates the hydrophone package from surface expression motion. Groups of DAISYs are able to localize some types of sounds, which could be helpful for attributing radiated noise to marine energy converters. The DAISY metadata streams (e.g., hydrophone depth, hydrophone motion) provides a rich diagnostic capability, as demonstrated in the interpretation of flow noise occurrences. Overall, the modular nature of the DAISY allows the general design to be easily modified for different environments.

Despite these capabilities, drifting hydrophones like the DAISY have several limitations. While deployment and recovery are feasible at almost any current speed as long as the vessel involved is drifting with the hydrophones, energetic wave environments can pose a significant risk to human safety. Because of this, drifting measurements around WECs may not be able to capture radiated noise that only occurs during elevated sea states. Second, drifting measurements are temporal snapshots that may not be able to identify longer-term changes in radiated noise or trends with marine energy converter operating state. Third, these types of measurements inherently involve relatively shallow receivers around what are expected to be relatively low-frequency acoustic sources. This will produce data that includes propagation effects like Lloyd's mirror, in which surface-reflected waves interact with direct path arrivals to cause constructive and destructive interference. These and other effects will be dependent on source characteristics including water depth, the frequency of radiated noise produced by marine energy converters, receiver depths, and other surface conditions. However, modulated signals created by marine energy converters and DAISY motion may prove beneficial in identifying and mitigating these effects. Finally, there are fewer commercially available drifting systems and those that do exist require more specialized knowledge to use effectively. Nonetheless, the ability to collect acoustic data at close range to marine energy converters without concern for flow noise makes drifting hydrophones effective tools for this use case. Finally, while developed for marine energy applications, DAISYs may be helpful for monitoring sound sources in energetic environments, including radiated noise from mining and marine construction.

Supplementary information. Supplementary information includes diagnostics from the 10 m tether test in Admiralty Inlet, a schematic of the reference hydrophone package, and sound speed profiles measured at WETS.

Acknowledgments. DAISY development and testing was supported by many individuals. The authors wish to acknowledge helpful contributions from the following individuals and institutions. From the University of Hawai'i, Kimball Millikan, Andreia Queima, Dan Fitzgerald, Keith Bethune, Nic Ulm, and Olivia Hughes helped to prep and deploy DAISYs at WETS. Pat Cross facilitated financial support for the project and advocated for DAISY testing at WETS. James Joslin (MarineSitu, Inc.) helped to support DAISY testing at WETS. From Sea Engineering, Tor Harris, Patrick Anderson, and Don Bunnell helped keep us safe on the water at WETS even when significant wave heights were "sporting". Jim Thomson (University of Washington) and Levi Kilcher (National Renewable Energy Laboratory) provided the ADVs used to characterize relative velocity and helped us interpret the measurement results. Shima Abadi (UW) provided helpful guidance on localization algorithm implementation. Finally, DAISY development benefited from the support of numerous researchers at Pacific Northwest National Laboratory including Emma Cotter, Joe Haxel, Garrett Staines, and last, but not least, John Vavrinec.

Availability of Data and Materials

DAISY design and manufacturing information can be accessed through pmec.us/research-projects/daisy. The data underlying the figures in this publication can be accessed through MHK-DR (https://mhkdr.openei.org/submissions/570).

Author Contributions

Conceptualization: BP, CB; Data Curation: BP, LJ; Formal Analysis: BP, LJ, CB; Funding Acquisition: BP; Investigation: BP, CC, GC, JN, PM, LJ, CB; Methodology: BP, CC, JN, GC; Project Administration: BP; Software: BP, CC, LJ, PM, CB; Supervision: BP, CB; Visualization: BP, LJ; Writing - Original Draft Preparation: BP, LJ; Writing - Review & Editing: BP, LJ, CC, GC, PM, LJ, CB.

Funding

The project was financially supported by the U.S. Department of Energy's Water Power Technology Office under DE-EE0007823, DE-FG36-08GO18180, DE-EE0008895 (TEAMER), and DE-EE0009959, as well as the U.S. Department of Defense's Naval Facilities Engineering Systems Command (NAVFAC) under N00024-08-D-6323, Task Order 0016, N00024-08-D-6323, Task Order 0033, and N00024-08-D-6323, Task Order N0002418F8804.

Ethics Declarations

Conflict of Interest

PM is currently employed by MarineSitu, Inc., which is involved in commercialization of the DAISY hardware and software. During DAISY development, PM was employed by the University of Washington.

Appendix A Flow Shield Attenuation

As discussed in Sec. 3, we initially experimented with foam and plastic shell flow shields that resulted in attenuation of propagating sound by > 10 dB at frequencies > 1 kHz. For the fabric flow shield, attenuation could be caused by reflection, either from air bubbles on the surface of the fabric or the fabric itself, or absorption by the flow shield materials. In addition, reflection from the spring steel tensioning rods and PVC guards is possible, though neither of these components shadow a significant proportion of the hydrophone element. However, quantitatively evaluating flow shield attenuation in situ is complicated by variations in received levels with spatial position (horizontal and vertical) due to differences in propagation and other environmental factors. Similarly, simulation of flow shield attenuation is complicated by a lack of definition for the the acoustic properties of the flow shield components. Here, we present a theoretical argument for limited attenuation by the fabric and compare this to in situ experiments with a controlled source and available field data from testing in currents in Admiralty Inlet, WA and in waves at WETS.

A.1 Theoretical Considerations

Estimating the transmission or attenuation of sound by a material like the flow shield fabric is complicated. Assuming the flow shield can be reasonably modeled as a thin layer between two fluid half spaces of salt water, the general solution for the transmission coefficient of sound at normal incidence through three media with constant cross sections is

$$T = \frac{2}{(1 + Z_1/Z_3)\cos(k_2 l) + j(Z_2/Z_3 + Z_1/Z_2)\sin(k_2 l)}, \tag{A1}$$

where Z represents the acoustic impedance of each medium, k_2 is the acoustic wavenumber in the second medium (flow shield fabric) and l is the thickness of that layer. In the case where $k_2 l \ll 1$, as is generally the case for the flow shield, given its thickness, the imaginary terms are negligible and the transmission coefficient simplifies to

$$T = \frac{2Z_3}{Z_1 + Z_3}. \tag{A2}$$

Here, $Z_1 = Z_3$ since the fabric is surrounded by water. This solution indicates that the layer becomes acoustically transparent at frequencies where the wavelength is much longer than the thickness of the layer (Blackstock, 2000). Even if the absorption coefficient of the fabric is extremely large (i.e., many dB per cm), sound will be transmitted through the interface without considerable decreases in intensity.

The flow shield's fabric is 84% polyester/16% spandex, ∼1 mm thick, and has a mass density of 0.21 kg/m^2. A literature review did not identify measurements for this specific material, but Samuel et al. (2021) measured single woven layers of polyester fabrics in an impedance tube and noted that they effectively transmitted incident sound below 5 kHz. Ultrasonic (1 MHz and higher) measurements of attenuation rates of polymers with acoustic properties similar to polyester yielded attenuation rates on the order of 1-10 dB/cm-MHz (Bloomfield et al., 2000). Assuming attenuation rates are comparable in the flow shield fabric, frequencies measurable by the DAISY hydrophones would be expected to attenuate by much less than 0.5 dB. Even if the attenuation rate in the fabric is considerably higher, we would expect attenuation to be limited due to the thickness of the material.

A.2 Controlled Experiment

The impact of the flow shield was evaluated through controlled experiments at the University of Washington's Acoustic Test Facility. This is a barge equipped with moon-pools and a hydraulic ram that allow a receiver and calibrated transducer (Navy Type 41) to be positioned at a range of 3.2 m and depth of 2.1 m. The transducer generated short-duration, high-amplitude tones from 10 kHz to 160 kHz in increments of 1 kHz. The lower frequency limit was set by transducer capabilities. At each frequency, three tones were generated and received levels were calculated by manually identifying the amplitude of the constant portion of the signal envelope. Comparisons were made between received levels on a reference hydrophone (icListen HF Geospectrum element) in an unshielded configuration and two shielded configurations: (1) spring steel rod centered on the transducer and (2) fabric panel centered on transducer. Results are shown in Fig. A1. When the transducer is centered on a fabric panel, we observe oscillatory patterns in the frequency response, typically less than 3 dB, that are centered around 0 dB at frequencies below 120 kHz. We attribute this to the interference patterns generated by scattering from the spring steel elements, which produce considerably more scattering when in line with the transducer. These measurements generally suggest that, in the field, sound produced by marine energy converters is unlikely to be significantly attenuated by the flow shield below 120 kHz, while at

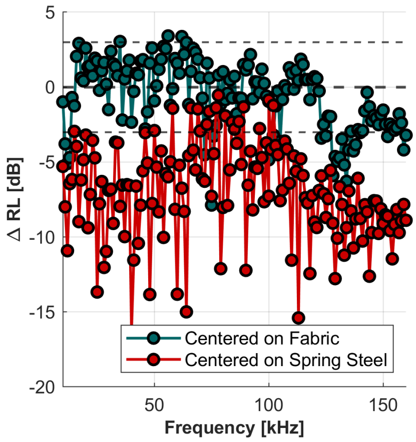

Fig. A1 Variation in received levels between a shielded and unshielded hydrophone as a function of frequency during controlled experiments Thin dashed lines denote a range of ± 3 dB.

higher frequencies attenuation of 3-5 dB may be expected. Since marine energy converters have not been generally found to produce sound at such high frequencies, this limited attenuation is unlikely to be of practical significance. Additional results from this experiment are included in Supplemental Information.

A.3 Field Data

During tether tests in Admiralty Inlet and at WETS, shielded and unshielded drifting hydrophones were deployed co-temporally. In Admiralty Inlet, received levels can be compared between the shielded DAISY, unshieled DAISY, and unshielded reference hydrophone. At WETS, received levels can be compared between the shielded DAISY and two unshielded DAISYs equipped with a heave plate. In each case, we consider the difference between median received levels for the frequency range between 1 kHz and the frequency at which ambient noise falls below the DAISY noise floor: 50 kHz in Admiralty Inlet and 20 kHz at WETS. In evaluating the results, if the flow shield materials reflect or absorb certain acoustic frequencies, we would expect consistent trends across tests and locations.

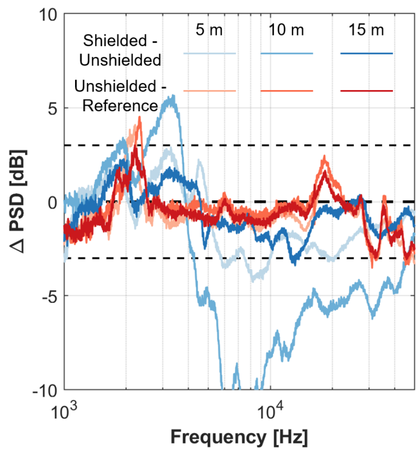

Fig. A2 Variation in median received levels between shielded DAISY, unshielded DAISY, and reference hydrophone in Admiralty Inlet for different tether lengths. Thin dashed lines denote a range of ± 3 dB.

Fig. A2 shows the differences in median received levels from the tether length tests in Admiralty Inlet. Negative values correspond to attenuation of propagating sound. For the 5 m and 15 m tether lengths, the variation between the shielded and unshielded DAISY is of similar magnitude to the differences between the unshielded DAISY and reference hydrophone, though the latter have more similar trends across tether lengths. For the 10 m tether length, the difference between the shielded and unshielded DAISY are much more significant, including higher received levels around 3 kHz. However, the inconsistency between tether lengths suggests this is not a consequence of flow shield construction and requires a different physical explanation. The outcomes from WETS (Fig. A3) are more straightforward to interpret. Here, the differences between the shielded and unshielded hydrophones rarely exceed 3 dB. However, as for tests in Admiralty Inlet, the differences between the shielded and unshielded DAISYs are more pronounced than differences between the two unshielded DAISYs (i.e., more consistent trends above 5 kHz for the pairs of unshielded DAISY).

Given that theoretical considerations and controlled experiments suggest that the flow shield is unlikely attenuate sound at frequencies $<$ 120 kHz, the most plausible

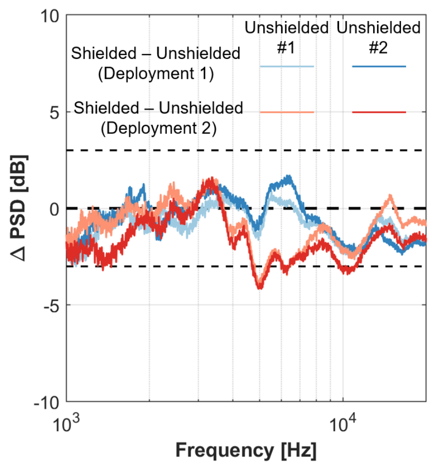

Fig. A3 Variation in median received levels between shielded and unshielded DAISYs at WETS. Thin dashed lines denote a range of ± 3 dB.

explanatory hypothesis for the intermittent, variable attenuation at lower frequencies is air bubbles on the shield surface or within the shield's enclosed volume. The DAISY fabric was specifically chosen for its ability to shed air bubbles upon immersion in benchtop tests. However, when we have positioned cameras (Go Pro Hero) inside the flow shield during field tests, we have observed that a limited number of small bubbles can remain adhered to the fabric. If a DAISY flow shield were to pass through the propeller wash from the deployment vessel, it is possible that the outer surface of the shield could retain a higher density of these small bubbles, resulting in scattering and absorption of incident sound. For example, bubbles with radii on the order of approximately 500 to 650 μm to would have relatively large scattering cross sections between 7-9 kHz (Medwin and Clay, 1998). This could be explain observed deviations between the shielded and unshielded hydrophones of ∼3 dB. However, based on extinction cross sections for bubbles, the concentration of bubbles required to significantly attenuate incident sound, as for the test with the 10 m tether in Admiralty Inlet, would be high in comparison to inferred bubble size distributions and attenuation reported from bubbles in vessel wakes (NRDC, 1946; Vagle and Burch, 2005). Nonetheless, it is possible that this represents an edge case where high concentrations of bubbles were entrained within the flow shield. The probability of this occurring would vary each time a DAISY is deployed and would be more likely at current sites, where the deployment vessel engines are often operating a relatively high power levels to maneuver. In addition to potentially corrupting the flow shield's acoustic properties, vessel wakes could also negatively impact measurements by injecting high volumes of bubbles that cause excess attenuation over the propagation path and generate a localized upward refracting environment (Vagle and Burch, 2005).

Overall, the balance of evidence suggests that the DAISY flow shield itself does not result in significant acoustic attenuation and that deviations from this are likely attributed to deployment approaches and could be mitigated with care. Furthermore, since no evidence indicates significant attenuation at frequencies below 2 kHz, where many marine energy converters are expected to radiate the most intense noise, the use of flow shields in currents remains recommended. Deployments involving combinations of shielded and unshielded drifting hydrophones could further reduce uncertainty at higher frequencies, as residual relative velocities for an unshielded, drifting hydrophone should be unaffected by flow noise at frequencies above a few hundred Hz (Bassett et al., 2014).

Appendix B Alternative Tethers in Currents

Because tether strum likely drives low-frequency (<20 Hz) self-noise from hydrophone package vibration, a comparison was made between rubber cord, low-stretch nylon cord, and a nylon cord faired to reduce vortex induced vibrations (Fig. B4). For these tests, DAISY hydrophone packages were equipped with flow shields and tether lengths of 5, 10, and 15 m were employed.

Performance across tether types and lengths are summarized in Fig. B5. In general, the nylon cord produced the highest amplitude vibration and the faired nylon cord the least. For unknown reasons, the rubber cord produced limited vibration for one drift (10 m tether length). During these tests, hydrophone packages on all tether types encountered significant depth excursions and tilt variations (Fig. B6), but the flow shield was universally effective in suppressing flow noise. In these conditions, unshielded hydrophones would likely have experienced high-intensity flow noise. Finally, we note that the reference hydrophone, which has a short, rigid element, does not experience vibratational self-noise at the same frequencies at the DAISYs (Fig. 6) despite being equipped with the same rubber tether.

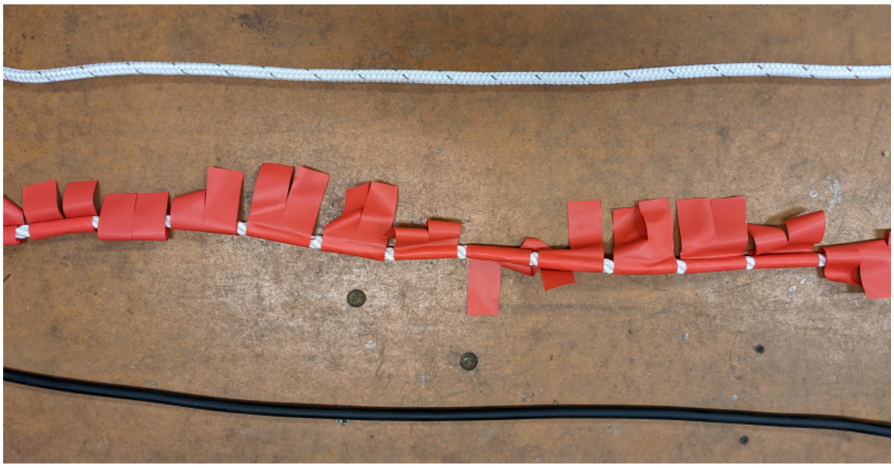

Fig. B4 (top) Low-stretch nylon cord, (middle) low-stretch nylon cord with vinyl tape fairing (3M 3903), (bottom) standard rubber cord. All cords are 9.53 mm (3/8 in) in diameter.

References

Abadi, S. H., Wacker, D. W., Newton, J. G., and Flett, D. (2019). Acoustic localization of crows in pre-roost aggregations. *The Journal of the Acoustical Society of America*, 146(6):4664–4671.

Amaral, J. L., Miller, J. H., Potty, G. R., Vigness-Raposa, K. J., Frankel, A. S., Lin, Y.-T., Newhall, A. E., Wilkes, D. R., and Gavrilov, A. N. (2020). Characterization of impact pile driving signals during installation of offshore wind turbine foundations. *The Journal of the Acoustical Society of America*, 147(4):2323–2333.

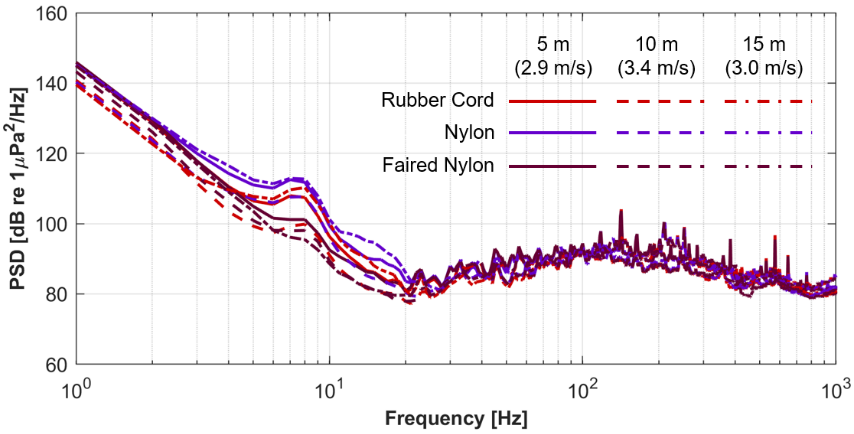

Fig. B5 Inter-comparison of median PSDs between DAISYs with different tether compositions and lengths in Admiralty Inlet (WA).

Bassett, C., Polagye, B., Holt, M., and Thomson, J. (2012). A vessel noise budget for Admiralty Inlet, Puget Sound, Washington (USA). *The Journal of the Acoustical Society of America*, 132(6):3706–3719.

Bassett, C., Thomson, J., Dahl, P. H., and Polagye, B. (2014). Flow-noise and turbulence in two tidal channels. *The Journal of the Acoustical Society of America*, 135(4):1764–1774.

Bassett, C., Thomson, J., and Polagye, B. (2013). Sediment-generated noise and bed stress in a tidal channel. *Journal of Geophysical Research: Oceans*, 118(4):2249–2265.

Bassett, C., Thomson, J., Polagye, B., and Rhinefrank, K. (2011). Underwater noise measurements of a 1/7 th scale wave energy converter. In *OCEANS'11 MTS/IEEE KONA*, pages 1–6. IEEE.

Biffard, B., Morgan, M., Muzi, L., Dakin, T., and Van Buren, P. (2022). An integrated hydrophone calibration system for ocean observing: ONC HydroCal. In *OCEANS 2022, Hampton Roads*, pages 1–5. IEEE.

Blackstock, D. (2000). *Fundamentals of Physical Acoustics*. Wiley-Interscience.

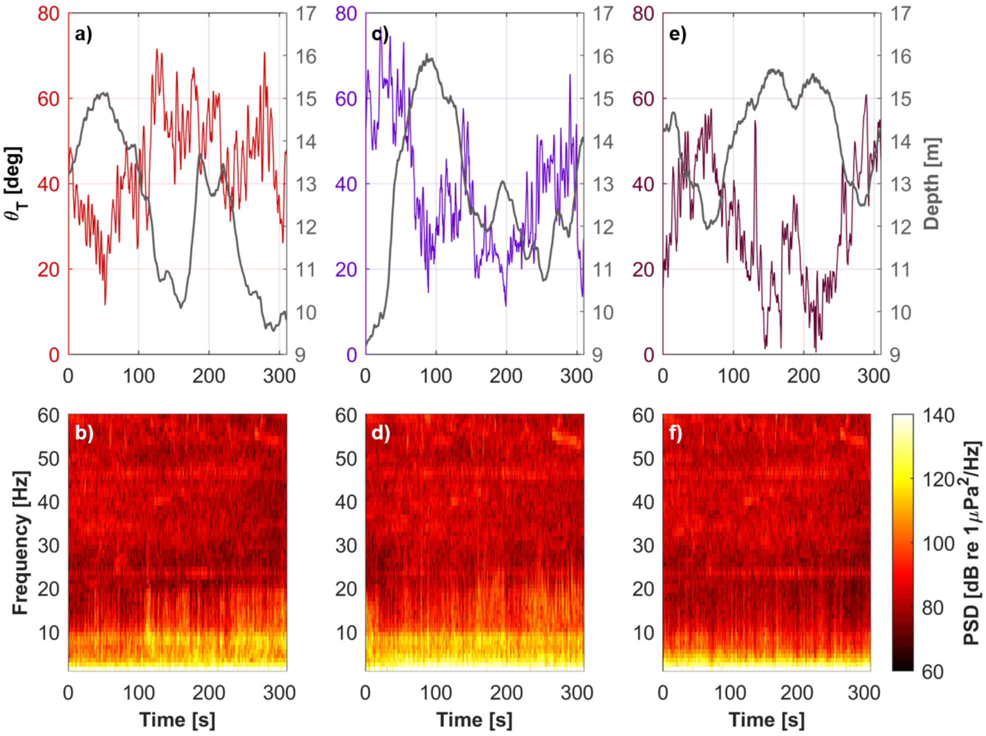

Fig. B6 Time series of hydrophone package tilt and hydrophone depth for flow-shielded DAISY with 15 m tether composed of (a) rubber, (c) nylon, and (e) faired nylon. Tilt coloration matches drifter configuration Fig. B5. Hydrophone depth is greater than the tether length due to the vertical extent of the surface expression and hydrophone package. (b,d,f) Low-frequency (0-60 Hz) spectrograms for the same. Persistent tether strum at 8 Hz is apparent for the rubber and unfaired nylon cord. Despite relatively large depth excursions and persistent tilt, the flow shields are effective at limiting flow noise.

Bloomfield, P., Lo, W.-J., and Lewin, P. (2000). Experimental study of the acoustical properties of polymers utilized to construct pvdf ultrasonic transducers and the acousto-electric properties of pvdf and p(vdf/trfe) films. *IEEE Transactions on Ultrasonics, Ferroelectrics, and Frequency Control*, 47(6):1397–1405.

Bruce Martin, S., Gaudet, B. J., Klinck, H., Dugan, P. J., Miksis-Olds, J. L., Mellinger, D. K., Mann, D. A., Boebel, O., Wilson, C. C., Ponirakis, D. W., et al. (2021). Erratum: Hybrid millidecade spectra: A practical format for exchange of long-term ambient sound data [jasa express lett. 1 (1), 011203 (2021)]. *JASA Express Letters*, 1(8):011203.

Buaka Muanke, P. and Niezrecki, C. (2007). Manatee position estimation by passive acoustic localization. *The Journal of the Acoustical Society of America*, 121(4):2049–2059.

Cato, D. H. (1998). Simple methods of estimating source levels and locations of marine animal sounds. *The Journal of the Acoustical Society of America*, 104(3):1667–1678.

Chang, G., Harker-Klimeš, G., Raghukumar, K., Polagye, B., Haxel, J., Joslin, J., Spada, F., and Staines, G. (2021). Clearing a path to commercialization of marine renewable energy technologies through public–private collaboration. *Frontiers in Marine Science*, 8:1180.

Compagnoni, M., Notari, R., Antonacci, F., and Sarti, A. (2014). A comprehensive analysis of the geometry of tdoa maps in localization problems. *Inverse Problems*, 30(3):035004.

Cotter, E., McVey, J., Weicht, L., and Haxel, J. (2024). Performance of three hydrophone flow shields in a tidal channel. *JASA Express Letters*, 4(1):016001–1–6.

Demirbilek, Z. and Vincent, C. (2002). *Water Wave Mechanics, Chapter II-1, Coastal Engineering Manual (EM 1110-2-1100).* U.S. Army Corp of Engineers.

Eaves, S. L., Staines, G., Harker-Klimeš, G., Pinza, M., and Geerlofs, S. (2022). Triton field trials: Promoting consistent environmental monitoring methodologies for marine energy sites. *Journal of Marine Science and Engineering*, 10(2):177.

Ehrenberg, J. E. and Steig, T. W. (2002). A method for estimating the "position accuracy" of acoustic fish tags. *ICES Journal of Marine Science*, 59(1):140–149.

Goring, D. G. and Nikora, V. I. (2002). Despiking acoustic doppler velocimeter data. *Journal of Hydraulic Engineering*, 128(1):117–126.

Hasselman, D. J., Hemery, L. G., Copping, A. E., Fulton, E. A., Fox, J., Gill, A. B., and Polagye, B. (2023). 'scaling up'our understanding of environmental effects of marine renewable energy development from single devices to large-scale commercial arrays. *Science of the Total Environment*, 904:166801.

Hawkins, A., Popper, A., Fay, R., Mann, D., Bartol, S., Carlson, T., Coombs, S., Ellison, W., Gentry, R., Halvorsen, M., et al. (2014). Sound exposure guidelines for fishes and sea turtles: A technical report. Technical report, Springer and ASA Press, Cham, Switzerland.

Haxel, J., Zang, X., Martinez, J., Polagye, B., Staines, G., Deng, Z. D., Wosnik, M., and O'Byrne, P. (2022). Underwater noise measurements around a tidal turbine in a busy port setting. *Journal of Marine Science and Engineering*, 10(5):632.

Holler, R. A. (2014). The evolution of the sonobuoy from world war ii to the cold war. *US Navy Journal of Underwater Acoustics*, 27:322–346.

IEC (2019). Iec/ts 62600-40; acoustic characterization of marine energy converters. Technical report, International Electrotechnical Commission.

Jensen, F. B., Kuperman, W. A., Porter, M. B., Schmidt, H., and Tolstoy, A. (2011). *Computational Ocean Acoustics*, volume 2011. Springer.

Konagaya, T. (1982). A new telemetric method of determining the positions of swimming fish. *Bulletin of the Japanese Society of Scientific Fisheries*, 48(11):1545–1550.

Lee, S., Kim, S.-R., Lee, Y.-K., Yoon, J. R., and Lee, P.-H. (2011). Experiment on effect of screening hydrophone for reduction of flow-induced ambient noise in ocean. *Japanese Journal of Applied Physics*, 50(7S):07HG02.

Lossent, J., Lejart, M., Folegot, T., Clorennec, D., Di Iorio, L., and Gervaise, C. (2018). Underwater operational noise level emitted by a tidal current turbine and its potential impact on marine fauna. *Marine Pollution Bulletin*, 131:323–334.

Macaulay, J., Gordon, J., Gillespie, D., Malinka, C., and Northridge, S. (2017). Passive acoustic methods for fine-scale tracking of harbour porpoises in tidal rapids. *The Journal of the Acoustical Society of America*, 141(2):1120–1132.

Martin, S. B., Gaudet, B. J., Klinck, H., Dugan, P. J., Miksis-Olds, J. L., Mellinger, D. K., Mann, D. A., Boebel, O., Wilson, C. C., Ponirakis, D. W., et al. (2021). Hybrid millidecade spectra: A practical format for exchange of long-term ambient sound data. *JASA Express Letters*, 1(1).

Medwin, H. and Clay, C. (1998). *Fundamentals of acoustical oceanography.* Academic Press.

Melikoglu, M. (2018). Current status and future of ocean energy sources: A global review. *Ocean Engineering*, 148:563–573.

NMFS (2018). 2018 revisions to: Technical guidance for assessing the effects of anthropogenic sound on marine mammal hearing (version 2.0): Underwater thresholds for onset of permanent and temporary threshold shifts. Technical report, Dept. of Commer., NOAA National Marine Fisheries Service, USA.

Pirotta, E., Fernandez Ajó, A., Bierlich, K., Bird, C. N., Buck, C. L., Haver, S. M., Haxel, J. H., Hildebrand, L., Hunt, K. E., Lemos, L. S., et al. (2023). Assessing variation in faecal glucocorticoid concentrations in gray whales exposed to anthropogenic stressors. *Conservation Physiology*, 11(1):coad082.

Polagye, B., Joslin, J., Murphy, P., Cotter, E., Scott, M., Gibbs, P., Bassett, C., and Stewart, A. (2020). Adaptable monitoring package development and deployment: Lessons learned for integrated instrumentation at marine energy sites. *Journal of Marine Science and Engineering*, 8(8):553.

Polagye, B. and Murphy, P. (2015). Acoustic characterization of a hydrokinetic turbine. In *Proceedings of the 11th European Wave and Tidal Energy Conference (EWTEC), Nantes, France.*

Polagye, B., Murphy, P., Cross, P., and Vega, L. (2017). Acoustic characteristics of the lifesaver wave energy converter. In *Proceedings of the 12th European Wave and Tidal Energy Conference (EWTEC), Cork, Ireland.*

Polagye, B. L. and Bassett, C. (2020). Risk to marine animals from underwater noise generated by marine renewable energy devices. In Copping, A. E. and Hemery, L. G., editors, *OES-environmental 2020 state of the Science report: Environmental effects of marine renewable energy development around the world. Report for ocean energy* *systems (OES)*, pages 67–85. Pacific Northwest National Lab.(PNNL), Richland, WA (United States).

Popper, A. N. and Hastings, M. C. (2009). The effects of human-generated sound on fish. *Integrative Zoology*, 4(1):43–52.

Raghukumar, K., Chang, G., Spada, F., and Jones, C. (2020). A vector sensor-based acoustic characterization system for marine renewable energy. *Journal of Marine Science and Engineering*, 8(3):187.

Richardson, W. J., Greene Jr, C. R., Malme, C. I., and Thomson, D. H. (2013). *Marine mammals and noise*. Academic Press.

Risch, D., Marmo, B., van Geel, N., Gillespie, D., Hastie, G., Sparling, C., Onoufriou, J., and Wilson, B. (2023). Underwater noise of two operational tidal stream turbines: A comparison. In *The Effects of Noise on Aquatic Life: Principles and Practical Considerations*, pages 1–22. Springer.

Risch, D., van Geel, N., Gillespie, D., and Wilson, B. (2020). Characterisation of underwater operational sound of a tidal stream turbine. *The Journal of the Acoustical Society of America*, 147(4):2547–2555.

Samuel, B. T., Barburski, M., Witczak, E., and Jasińska, I. (2021). The influence of physical properties and increasing woven fabric layers on the noise absorption capacity. *Materials*, 14(20).

Sousa-Lima, R. S., Norris, T. F., Oswald, J. N., and Fernandes, D. P. (2013). A review and inventory of fixed autonomous recorders for passive acoustic monitoring of marine mammals. *Aquatic Mammals*, 39(1):23–53.

Spiesberger, J. L. and Fristrup, K. M. (1990). Passive localization of calling animals and sensing of their acoustic environment using acoustic tomography. *The American Naturalist*, 135(1):107–153.

Stokes, G. G. (1851). On the effect of the internal friction of fluids on the motion of pendulums. *Transactions of the Cambridge Philosophical Society*, 9:8.

Strasberg, M. (1979). Nonacoustic noise interference in measurements of infrasonic ambient noise. *The Journal of the Acoustical Society of America*, 66(5):1487–1493.

Taylor, G. (1937). The statistical theory of isotropic turbulence. *Journal of the Aeronautical Sciences*, 4(8):311–315.

Tenorio-Hallé, L., Thode, A. M., Lammers, M. O., Conrad, A. S., and Kim, K. H. (2022). Multi-target 2d tracking method for singing humpback whales using vector sensors. *The Journal of the Acoustical Society of America*, 151(1):126–137.

Thomson, J. (2012). Wave breaking dissipation observed with "swift" drifters. *Journal of Atmospheric and Oceanic Technology*, 29(12):1866–1882.

Thomson, J., Polagye, B., Durgesh, V., and Richmond, M. C. (2012). Measurements of turbulence at two tidal energy sites in Puget Sound, WA. *IEEE Journal of Oceanic Engineering*, 37(3):363–374.

Tougaard, J., Hermannsen, L., and Madsen, P. T. (2020). How loud is the underwater noise from operating offshore wind turbines? *The Journal of the Acoustical Society of America*, 148(5):2885–2893.

United States Office Of Scientific Research And Development. National Defense Research Committee, Issuing Body (1946). *The Physics of Sound in the Sea.* ashington, D.C.: Office of Scientific Research and Development, National Defense Research Committee, Division 6.

Vagle, S. and Burch, H. (2005). Acoustic measurements of the sound-speed profile in the bubbly wake formed by a small motor boat. *The Journal of the Acoustical Society of America*, 117(1):153–163.

Wahlberg, M., Møhl, B., and Teglberg Madsen, P. (2001). Estimating source position accuracy of a large-aperture hydrophone array for bioacoustics. *The Journal of the Acoustical Society of America*, 109(1):397–406.

Watkins, W. A. and Schevill, W. E. (1972). Sound source location by arrival-times on a non-rigid three-dimensional hydrophone array. *Deep Sea Research*, 19(10):691–706.

Wilson, B., Lepper, P. A., Carter, C., and Robinson, S. P. (2014). Rethinking underwater sound-recording methods to work at tidal-stream and wave-energy sites. In *Marine Renewable Energy Technology and Environmental Interactions*, pages 111–126. Springer.